Improved antifouling performance of polyester thin film nanofiber composite membranes prepared by interfacial polymerization

P. Arribas, M.C. García-Payo, M. Khayet, L. Gil

PII: S0376-7388(19)33455-6

DOI: https://doi.org/10.1016/j.memsci.2019.117774

Reference: MEMSCI 117774

To appear in: *Journal of Membrane Science*

Received Date: 11 November 2019

Revised Date: 18 December 2019

Accepted Date: 20 December 2019

Please cite this article as: P. Arribas, M.C. García-Payo, M. Khayet, L. Gil, Improved antifouling performance of polyester thin film nanofiber composite membranes prepared by interfacial polymerization, *Journal of Membrane Science* (2020), doi: https://doi.org/10.1016/j.memsci.2019.117774.

CRediT author statement

Paula Arribas: Conceptualization, Methodology, Validation; Investigation, Data Curation, Writing-Original Draft,

María Carmen García-Payo: Conceptualization, Methodology, Writing-Review & Editing, Funding acquisition

Mohamed Khayet: Conceptualization, Methodology, Writing-Review & Editing, Funding acquisition

Luís Gil: Conceptualization, Supervision, Writing-Review & Editing

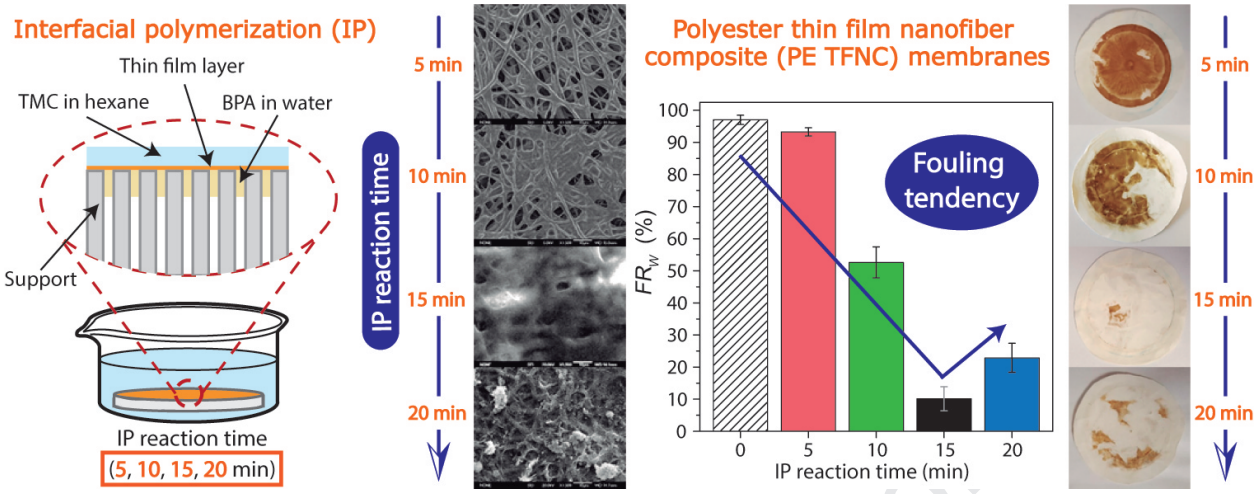

Improved antifouling performance of polyester thin film nanofiber composite membranes prepared by interfacial polymerization

P. Arribas[1,2,*], M.C. García-Payo[2], M. Khayet[2,3,*], L. Gil [4]

[1]Campus of International Excellence, Moncloa Campus (UCM-UPM), Madrid (Spain).

[2]Department of Structure of Matter, Thermal Physics and Electronics, Faculty of Physics, University Complutense of Madrid, Avda. Complutense s/n, 28040, Madrid (Spain).

[3]Madrid Institute for Advanced Studies of Water (IMDEA Water Institute), Calle Punto Com Nº 2, 28805, Alcalá de Henares, Madrid (Spain).

[4]Genetics and Eco-Physiology Research Group, School of Forest Engineering, University Polytechnic of Madrid, Avda. Complutense s/n, 28040, Madrid (Spain).

* Corresponding author: khayetm@fis.ucm.es

Tel. +34-91-3945185

Fax. +34-91-3945191

Abstract

Membrane technology is becoming increasingly important to solve the global water scarcity problem because it allows an efficient, economic and environmental friendly treatment of water. However, the long-term use of a filtration membrane is limited by fouling, which reduces water production rates and increases energy consumption. In this paper, polyester thin film nanofiber composite (PE TFNC) membranes with improved antifouling performance were developed for wastewater treatment. The membranes were prepared by interfacial polymerization (IP) of bisphenol A (BPA) and trimesoyl chloride (TMC) on the surface of polysulfone electrospun nanofiber membranes (PSU ENMs). The antifouling properties of the membranes were improved by varying the polymerization reaction time. All membranes were characterized with scanning electron microscope (SEM), attenuated total reflectance-fourier transform infrared spectroscopy (ATR-FTIR), porometry and zeta potential measurements. Humic acid (HA) permeation tests were carried out to relate their physicochemical properties to their filtration and antifouling performance. The best PE TFNC membrane (polymerized for 15 min) was compared with polyester based thin film composite membranes prepared on other supports and polyamide based thin film composite membranes formed by IP of piperazine (PIP) and TMC in the presence of trimethylamine (TEA). The best PE TFNC membrane exhibited a permeability of 213.0 $L/m^2h.bar$, two orders of magnitude greater than previously reported PE thin film composite membranes, a HA separation factor of 72.5% and an irreversible fouling factor of 10.2%.

Keywords: Electrospun nanofibrous membrane; Interfacial polymerization; Polyester; Polyamide; Thin film composite; Antifouling; Wastewater treatment.

1. Introduction

Membrane filtration technology has demonstrated extensive practical applications in separation processes such as water purification, wastewater treatment and seawater desalination. The numerous advantages of membrane technology in filtration applications include the low cost, high efficiency, simplicity, insignificant chemical consumption and environmental friendliness [1]. However, the main obstacle that restricts the application of membranes in water treatment is membrane fouling, which usually lowers the water productivity, deteriorates membrane separation capability (i.e. reduction of the permeate quality), shortens membrane lifespan and consequently, increases the operation and maintenance costs [1-4]. Fouling originates from the interaction between a membrane surface and foulant(s), thus, it is strongly influenced by the physicochemical properties of the membrane surface such as pore size and its geometry, charge density, roughness and hydrophilicity [3-6]. Therefore, it is of a great importance to design and develop new membranes with optimized surface properties to reduce fouling in order to overcome the aforementioned limitations.

Interfacial polymerization (IP) is an effective membrane surface modification technique widely used to improve both the filtration and antifouling performance of membranes [2, 3, 5-10]. After IP, the resulting thin film composite (TFC) membrane is comprised of a thin polymeric active layer on top of a porous supporting membrane. The key advantage of the TFC approach is the possible separate optimization of the active layer and the support layer to get membranes with high filtration performance. Most of the research studies have been focused on: i) optimizing the physicochemical properties of the TFC active layer to improve the permeability, selectivity and antifouling capacity of the resulting membranes [11-17], and ii) improving the intrinsic morphological structure and chemical properties of the support layer suitable for the

active layer formation with enhanced mechanical strength and low resistance to permeate flow [18-25].

Several parameters are involved in the IP procedure like the monomer type and its concentration in the aqueous and the organic phases, the used additives in both phases and the polymerization reaction time. It was shown that the IP reaction time plays an important role in determining the structural morphology and composition of the active layer as it affects the extent of polymerization and thus the density and thickness of the active layer [14, 16, 26-30]. Different types of water-soluble monomers have been considered such as the commonly used polyamines to form polyamide (PA) TFC membranes [10-16, 24-28] and the less used polyols or polyphenols to form polyester (PE) TFC membranes [7-9, 31, 32]. These last membranes exhibit higher antifouling performance against hydrophobic contaminants because of their abundant surface hydroxyl groups, whereas PA TFC membranes have better salt rejection properties due to their highly cross-linked structure**.** For instance, PE TFC membrane prepared by IP using tannic acid (TA) and trimesoyl chloride (TMC) on a porous polyethersulfone (PES) ultrafiltration (UF) support [8] exhibited 56% greater water permeability (*PWP* = 23.4 L/m^{2}h.bar) and much better antifouling capacity against humic acid (HA) (i.e. lower irreversible fouling factor, FR_W = 1%) than that of a PA TFC membrane prepared by IP of piperazine (PIP) and TMC on a PES UF support (*PWP* = 10.3 L/m^{2}h.bar and FR_W = 48%, respectively) [6]. However, the salt rejection of $MgSO_4$ of the PE TFC membrane (50.2%) was lower than that of the PA TFC membrane (97.4%).

The most common used porous supports to develop the TFC membranes are commercial microfiltration (MF) and UF membranes or lab-made membranes prepared by the phase inversion method, which usually have a low surface porosity [33]. Polysulfone (PSU) [3-5, 15-17] and PES [6-8, 11-13] are the most employed supporting

materials, mainly due to their low price, ease of processing, and good chemical, thermal and mechanical resistance. Recently, electrospun nanofiber membranes (ENMs) were successfully used as an alternative support to fabricate TFC membranes [22, 33-35]. Compared with the conventional MF/UF supporting membranes, ENMs offer unique advantages such as a higher porosity, an interconnected nanofiber structure with an open pore morphology and a larger surface area to volume ratio, a low flow resistance and a high permeability. The resulting thin film nanofiber composite (TFNC) membranes exhibited significantly higher permeation fluxes and comparable rejection factors than the commercial nanofiltration (NF) membranes and conventional TFC membranes. For instance, the PA TFNC membrane developed by Yung et al. [33] achieved a superior filtration performance over a conventionally prepared PA TFC membrane, with a salt rejection factor of 99.1% and a permeation flux about 2 times higher than that of the PA TFC membrane having a salt rejection factor of 97.3%. Recently, Kaur et al. [34] reported PA TFNC membranes with up to 256% larger permeate fluxes than those of commercial NF membranes and only 8–12% lower salt rejection factors. Compared to PA TFNC membranes, very few studies have been reported on the development of PE TFNC membranes.

In the present study, PE TFNC membranes were prepared by IP of bisphenol A (BPA) and TMC. The effects of the polymerization reaction time on the antifouling performance and the physicochemical properties of the PE TFNC membranes were studied and the optimum IP reaction time was determined. Furthermore, the formation process of the PE layer was elucidated by means of FTIR spectra. PE layers were also prepared on different supports under the optimum IP conditions to investigate the influence of the supporting membrane on the physicochemical properties, the filtration performance and the antifouling capacity of the resulting PE TFC membranes. Different

PA TFC membranes were also prepared by IP reaction of piperazine (PIP) and TMC in the presence of the acid acceptor trimethylamine (TEA) and their filtration and antifouling performance was compared to that of the PE TFC membranes. New insight on the formation of the PE thin film layer on ENMs was emphasized in this study showing the relationship between the polymerization reaction time and the physicochemical, filtration and antifouling properties of the PE TFNC membranes.

2. Materials and methods

2.1. Materials

The spinning solution was prepared from the polymer polysulfone (PSU, UDEL P-3500 LCD, Solvay Specialty Polymers; Mw = 79,000 g/mol; ρ = 1.24 g/cm^3) and a mixture of the solvents *N*, *N*-dimethyl formamide (DMF, Sigma-Aldrich) and tetrahydrofuran (THF, Sigma-Aldrich). The monomer trimesoyl chloride (TMC, Sigma-Aldrich) and the solvent hexane (Sigma-Aldrich, puriss., ≥99% (GC)) were used to prepare the organic phase for the modification of the surface of the membranes by interfacial polymerization (IP). For the aqueous phase, the monomers bisphenol A (BPA, Sigma-Aldrich), m-phenylenediamine (MPD, Sigma-Aldrich), triethylamine (TEA, Sigma-Aldrich), piperazine (PIP, Sigma-Aldrich) and polyvinyl acetate (PVA, Sigma-Aldrich) were used either separately or combined to form a polyester (PE) or polyamide (PA) layer on the membrane surface. The organic foulant humic acid (HA, Fluka) having a molecular weight of 4.1 kDa was employed to prepare the feed solution of the filtration tests. Sodium hydroxide (NaOH, Panreac) was used to prepare a standard HA concentrated solution of 1 g/L. Hydrochloric acid (HCl, Sigma-Aldrich) was used to adjust to 11 the pH of the HA feed solution of 15 mg/L. Isopropyl alcohol (IPA, Sigma-Aldrich) was used to determine the void volume fraction (ε) of the membranes. POREFIL®, a fluorinated hydrocarbon (chemical nature: perfluoro-ether,

surface tension: 16 mN/m, vapor pressure: 3.33 Pa; viscosity: 4.4 mPa·s, POROMETER), was used as a wetting liquid to perform the pore size measurements. Commercial polyethersulfone (PES) microfiltration (MF) membrane (HPWP, hydrophilic, Millipore) was used as a support.

2.2. Preparation of PSU ENMs

The spinning solution was prepared by dissolving 20 wt.% PSU into the solvent mixture DMF/THF (80/20 wt.%). The solvent mixture with PSU was kept at 60ºC and stirred at 80 rpm for 10 h until the polymer was completely dissolved and the solution became homogeneous. The PSU electrospun solution had 35.8 ± 1.8 mN/m surface tension, 485.3 ± 0.8 mPa·s viscosity and 9.12 ± 0.15 μS/cm electrical conductivity at 25°C. More details can be found elsewhere [36].

Electrospinning was applied to prepare the PSU ENMs using the system described elsewhere [37, 38]. All PSU ENMs were prepared under the optimum electrospinning parameter conditions [37]: a polymer solution flow rate of 2.5 mL/h, an electric voltage of 16 kV, an air gap of 10 cm and an electrospinning time of 45 min. The electrospinning ambient conditions were kept in the ranges 20-25ºC and 38-41% relative humidity.

After electrospinning, PSU ENMs had a silky, fluffy and loose structure, which required delicate handling. Several studies [36, 37, 39-41] demonstrated the importance of the application of a heat post-treatment (HPT) on ENMs to improve their structural integrity, mechanical stability and filtration performance. Thus, in this study, two different conditions of the HPT were carried on the PSU ENMs after electrospinning. The PSU ENMs were treated either for 75 min at 230 ºC (ENM1) or for 120 min at 220 ºC (ENM2) (see Table 1). These were the optimized conditions resulting in very high filtration performances in our previous study [36].

2.3. Preparation of polyester and polyamide thin film composite membranes

IP is based on the formation of a dense polymeric top layer (thin film composite) on the membrane surface (support) as a result of the reaction between two monomers at the interface of two immiscible solvents (i.e. aqueous and organic phases). In this study, IP was employed to prepare polyester (PE) and polyamide (PA) thin film composite (TFC) membranes. Figure 1 shows a schematic illustration of the process: 1) the supporting membrane was immersed for 60 min in an aqueous solution containing a reactive monomer; 2) the soaked membrane was taken out from the aqueous solution and positioned vertically for 2 min to drain the excess of monomer on its surface; 3) the membrane was then dipped for 5, 10, 15 or 20 min in a second solution containing 0.25% w/v TMC in hexane; 4) the soaked membrane was extracted from the organic solution and drained vertically for 1 min; 5) finally, the membrane was dried in open-air for 24 h before characterization. All these steps were carried out at room temperature (~23ºC).

In this study, the monomers BPA and TMC were used to form a dense and thin layer of PE on the membrane surface, whereas the combination of monomers PIP and TMC in presence of the acid acceptor TEA was used to form a PA thin film on the membrane surface. Figure 2 shows the schematic reaction mechanisms of these different IP approaches. The thin film layers were formed on the prepared PSU ENMs (i.e. TFNC) and on PES commercial membranes (i.e. TFC) for sake of comparisons. Table 2 summarizes the preparation conditions of all developed membranes in this study.

2.4. Membranes characterization

The average thickness of the unmodified supporting membranes and its standard deviation were calculated from 41 different points measured along the membrane surface using a micrometer equipped with a feeler (ISL Isocontrol).

The water contact angles (θ_w) of the unmodified supporting membranes were measured at room temperature using a CAM100 device (Sb) with the Cam200usb software, which was used to acquire photographs of the water drop on the sample surface and to calculate the contact angle value. A Hamilton stainless steel needle was used to control the volume of the drops, which ranged between 12 and 14 μL. For each ENM sample at least 10 different drops were considered to determine the average value of the θ_w together with its standard deviation.

The void volume fraction (porosity ε) of all unmodified ENM supporting membranes was determined by measuring the density of the polymer material (ρ_{pol}) using isopropyl alcohol (IPA), which penetrates into the pores, and the density of the membrane (ρ_m) using distilled water, which does not go into the pores, according to equation (3) [42].

$$\varepsilon\,(\%) = \left(1 - \frac{\rho_m}{\rho_{pol}}\right) \cdot 100 \qquad (3)$$

The surface morphology of the membranes was analyzed by a field emission scanning electron microscope (FESEM, JEOL Model JSM-6335F) operated at 5 kV. Before conducting the SEM analysis, a thin gold layer of about 5 nm was sputtered on the membrane surface using an evaporator (EMITECH K550 X) for one minute under 25 mA. SEM images were evaluated with the software UTHSCSA Image Tool 3.0 to measure the diameter of the nanofibers of the PSU ENMs. At least 3 SEM images/per ENM sample were considered and the diameters of a total number of 100 nanofibers/per image were measured. Statistical analysis was used to determine the nanofiber diameter distribution (i.e. nanofiber diameter histogram) and to estimate the arithmetic weighted mean of the nanofiber diameters ($\overline{\lambda_w}$) with its corresponding weighted standard deviation ($\overline{s_w}$). More details can be found elsewhere [36].

The pore size of the membranes (i.e. inter-fiber space for ENMs, d_f) was measured at room temperature (~23ºC) with the capillary flow porometry method using a gas–liquid displacement Porometer (POROLUX™ 100, Porometer). POREFIL® (Porometer) was employed as the wetting liquid agent and compressed air as the inert gas. The applied hydrostatic pressure was varied in the range 0 – 0.45 MPa. At least 3 tests were performed for each membrane. The mean pore size ($\bar{d}_f$), the pore size distribution or differential filter flow (*DFF*) and the cumulative filter flow distribution (*CFF*) of the membranes were determined using the wet and dry curves.

The chemical structure of the membranes was analysed by Attenuated Total Reflectance Fourier Transform Infrared (ATR-FTIR) spectroscopy with a Nicolet device (Magna-IR 750 Series II) equipped with the detector DTGS-KBr (sulfate triglycerin deuterated with KBr window), a beam splitter KBr and an infrared source (Ever-Glo). The H-ATR Multiple Bounce (Spectra Tech) accessory with a ZnSe crystal and 13 steps was used for analysis. ATR-FTIR measurements were carried out at 128 scans and 8 cm^{-1} resolution.

The surface charge characteristics of the membranes were measured using a SurPASS streaming potential analyzer (Anton Paar GmbH, Austria). The Zeta potential (ζ-potential) measurement was carried out at 25 ± 2 ºC using 1 mM KCl solution as background electrolyte at a pH 10.0 ± 0.2 adjusted with a 0.1 M NaOH solution. For each measurement, two membrane samples with dimensions 20 × 10 mm^2 were placed into the measuring cell. The gap of the flow channel between their surfaces was set at 100 µm. Before starting the measurement, the samples were thoroughly rinsed with the measuring electrolyte. Three measurements were performed for each membrane to determine the mean and the standard deviation of the ζ-potential.

240 **2.6. Filtration experiments**

241 A crossflow experimental device previously designed in our research group was used
242 for the filtration tests [37]. Before carrying out the filtration tests, all membranes were
243 compacted by circulating distilled water for 3 h at a transmembrane pressure (ΔP) of
244 $3x10^5$ Pa. Distilled water was used first as feed for 1 h and the pure water permeability
245 (PWP) of the membranes was determined at a transmembrane pressure of 10^5 Pa. The
246 effective filtration area of the membrane was 21.76 ± 0.01 cm^2 and the feed solution
247 was circulated at a constant flow rate of 1.6-1.8 L/min. Subsequently, filtration test was
248 conducted using a HA solution of 15 mg/L at pH 11 (~23ºC) as feed for 7 h (*i.e.*, HA
249 test). Then, the filtration system was washed with distillated water without removing the
250 membrane and distilled water was circulated again for 1 h.

251 During each step, the produced permeate was measured as a function of time by
252 weighing the permeate in discrete time steps on an electronic balance (AND GF-1200).
253 The permeate fluxes of the HA solution (J_{HA}) and distilled water before (J_{w_0}) and after
254 (J_{w_f}) the HA filtration test were calculated from the measured mass (m) collected over a
255 period of time (Δt) as:

$$J\ (kg/m^2h) = \frac{m}{A_{ef}\Delta t} \tag{4}$$

256 where A_{ef} is the effective filtration area of the membrane.

257 The irreversible fouling factor (FR_W) was used to evaluate the antifouling
258 performance of the membranes. This was calculated in terms of pure water flux
259 reduction [43]:

$$FR_W\ (\%) = \frac{J_{w_0} - J_{w_f}}{J_{w_0}} \cdot 100 \tag{5}$$

260 Permeate, retentate and feed samples were extracted from the filtration system during
261 the HA test and a spectrophotometer (UV/VIS 7315, Jenway) was used to determine

their HA concentration at 254 nm wavelength. These values were used to calculate the separation factor (α) of the membranes as follows:

$$\alpha\ (\%) = \left(1 - \frac{2C_p}{C_r + C_f}\right) \cdot 100 \quad (6)$$

where C_p, C_r and C_f are the HA concentration of the permeate, retentate and feed solutions, respectively.

The filtration performance of the membranes was evaluated by means of the performance index (*PI*), which takes into account the final values of the HA permeate flux (J_{HA_f}) and the HA separation factor (α_f) obtained at the end of the HA test:

$$PI(kg/m^2h) = \frac{J_{HA_f} \cdot \alpha_f}{100} \quad (7)$$

3. Results and discussions

3.1. Polyester thin film nanofiber composite membranes prepared with different polymerization reaction times

The polymerization reaction time strongly affects the physicochemical properties of the developed thin film layer (*e.g.*, surface morphology, roughness, chemical structure and hydrophilicity) as it significantly influences the degree of polymerization and therefore, the thickness and the crosslinking density of the thin film [7, 9, 14, 16, 26-30]. In this study, the effects of the IP reaction time (t_{IP}) on the physicochemical properties, the antifouling capacity (irreversible fouling factor) and the filtration performance (water permeability, permeation fluxes and separation factor) of polyester thin film nanofiber composite (PE TFNC) membranes were investigated. In our previous work [36], a systematic study of the heat post-treatment applied to PSU ENMs was conducted to optimize their morphological structure and obtain membranes with improved filtration performance (i.e. up to 38% better filtration performance than that of commercial PES MF membranes). Those heat-treated optimized PSU ENMs were used

in this study as supporting membranes to prepare the PE TFNC membranes. The fabrication conditions, morphological properties and pure water permeability (*PWP*) of the supporting membranes are summarized in Table 1. ENM1 was the supporting membrane used in this section. A thin PE layer was formed on the membrane surface by reacting the monomers BPA and TMC with varying reaction times as described in the Materials and Methods section. The surface modified membranes were named according to the IP reaction time: PE TFNC1_5 (t_{IP} = 5 min), PE TFNC1_10 (t_{IP} = 10 min), PE TFNC1_15 (t_{IP} = 15 min) and PE TFNC1_20 (t_{IP} = 20 min) (see Table 2).

3.1.1. Effects of the polymerization reaction time on the physicochemical properties of polyester thin film nanofiber composite membranes

SEM images of the surface morphologies of the unmodified supporting membrane and the surface modified PE TFNC membranes are shown in Figure 3A. The polymerization time clearly affected the surface morphology of the resulting PE TFNC membranes. Before IP, the surface of the ENM1 support was rough due to its nanofiber structure. During the first 15 min of polymerization, the thickness of the formed PE layer increased with time and the inter-fiber space of the membrane was progressively covered with the PE film (PE TFNC1_5, PE TFNC1_10) leading to a less rough membrane surface until almost the entire surface of the membrane was covered by a smooth PE layer (PE TFNC1_15). When increasing the IP reaction time over 15 min (PE TFNC1_20), the PE layer became rougher with nodular structure and without any visible open inter-fiber space (see also Figure S1). Other authors [14, 16, 27, 28, 44] observed the increase of both the roughness and thickness of the top layer of thin film composite (TFC) membranes as a function of the polymerization reaction time.

The SEM observed morphological differences between the unmodified supporting membrane and the surface modified PE TFNC membranes explained the measured size

of the inter-fiber space of the membranes and its distributions (Figure 3B-C). Increasing the IP reaction time resulted in a left shift of both the cumulative (*CFF*) and normalized differential (*DFF*) inter-fiber space distributions of the membranes along with a decrease of their mean size of the inter-fiber space ($\overline{d_f}$) (see also data in Table 3). The $\overline{d_f}$ value of the surface modified membranes decreased by up to 74.3% with respect to that of the unmodified membrane. This reduction was significantly greater for 20 min of reaction time, which is likely related to the previously mentioned structural change of the formed PE thin film (i.e. from thin and smooth to thick and rough). Seman et al. [45] reported a similar left shift of the pore size distribution curves with a decrease of the mean pore size up to 45.6% for surface modified BPA TFC and tetramethyl BPA TFC membranes compared to the unmodified membrane.

Figure 3D displays the FTIR spectra of the unmodified supporting membrane, the surface modified PE TFNC membranes, BPA and TMC. In addition, Table 4 [5, 6, 9-13, 16-18, 20, 29, 46-50] provides the corresponding peak assignments of the IR bands. For the FTIR spectrum of the ENM1 support, the bands at 1322 and 1148 cm^{-1} showed the asymmetric and symmetric stretching vibration of S=O bonds of the base polymer PSU. Other characteristic strong IR bands of PSU substrate appeared at 1584, 1486 and 1237 cm^{-1}, which correspond to the C=C aromatic in-plane ring stretching vibration, the C‑H stretching vibration of the methyl group (CH_3‑C‑CH_3), and the C‑O‑C asymmetric stretching of aryl‑O‑aryl group, respectively. In addition, the two weak bands at 1387 and 1364 cm^{-1} are assigned to the presence of methyl groups in the PSU matrix.

The PE TFNC membranes exhibited a weak adsorption peak at about 1612 cm^{-1} and large peaks at 1509 and 832 cm^{-1}, which are likely due to the presence of excess BPA in the membranes (see FTIR spectrum of BPA). The presence of absorption peaks at 1612

and 1509 cm^{-1} was attributed to the C=C aromatic stretching vibrations of the ring of the BPA moiety [51]. Beside the PSU bands of the substrate and BPA, the spectrum of the PE TFNC membranes exhibited absorption peaks at 1720 and 1200 cm^{-1}, which correspond to C=O and C‑O stretching vibrations of the ester groups, respectively. The presence of these peaks verified the successful formation of the PE thin film layer on top of the ENM1 support for all IP reaction times. Additionally, a broad adsorption peak appeared in the range 3150 – 3700 cm^{-1} with a center at ~3355 cm^{-1} due to the stretching vibration of the hydroxyl groups (–OH), which could arise from the unreacted hydroxyl groups of BPA in the membranes as well as from the partial hydrolysis of the acyl chloride unit of TMC.

The FTIR spectrum of the membrane PE TFNC1_20 differed from that of the rest of the modified membranes. The changes in the peak corresponding to the C=O stretching vibration of the ester group at 1720 cm^{-1} (i.e. became broader due to a new contribution centered at 1698 cm^{-1}), the appearance of a broad contribution in the range 2300–2700 cm^{-1} and a narrow peak at 3110 cm^{-1} revealed the presence of carboxylic acid group (see Figure S2-A). In addition, the centre of the broad adsorption peak attributed to the stretching vibration of the –OH groups shifted to higher wavenumbers (3396 cm^{-1}). All this confirmed the change in the chemical structure of the membrane as it will be explained later on.

The analysis of the areas under the peak at 1720 cm^{-1} attributed to the –C=O group (i.e. CO bonding) and under the peak at 3355 cm^{-1} corresponding to the –OH group (i.e. OH bonding) and their ratio as a function of the IP reaction time can be used to explain the process of monomer crosslinking and film growth on the membrane surface (Figure 4 A-C). The intensity of the peak attributed to the –C=O group increased continuously with the reaction time (Figure 4A), indicating that both the film thickness and the

degree of crosslinking of the membrane layer increased with the reaction time [16, 26-28]. The intensity of the peak corresponding to the –OH group also increased with IP reaction time from 5 to 15 min (Figure 4B), but it was slower than that of the –C=O group, so that their ratio (OH/CO) decreased as plotted in Figure 4C. This behaviour can be explained based on the corresponding SEM images. At the beginning of the IP process, BPA molecules could freely diffuse through the organic phase, facilitated by the loose and open pore structure of the membrane, and react with TMC forming the initial PE film (PE TFNC1_5 in Figure 3A). The number of BPA molecules available for IP reaction was so large that only part could react with TMC increasing the amount of polyester bonds (–C=O) in the PE film with time while the rest remained un-reacted. The hydroxyl groups of the un-reacted BPA caused the increase with time of the intensity of the peak corresponding to the –OH bonds.

The diffusion of BPA towards TMC slowed down with increasing polymerization time due mainly to the continuous growth of the PE layer that progressively covered the inter-fiber space at the surface of the membrane (PE TNFC1_10 and PE TFNC1_15 in Figure 3A) and acted as barrier limiting BPA diffusion [14, 16, 52]. Over 15 min reaction time, the entire surface of the membrane was so covered by the PE film (PE TFNC1_20 in Figure 3A) that hindered the diffusion of BPA, which is confirmed by the reduction of the intensity of the peaks corresponding to pure BPA (1612, 1509 and 832 cm^{-1}) in the FTIR spectrum of the membrane PE TFNC1_20. At this stage of the IP process, two reactions occurred simultaneously: i) TMC reacted with the previously un-reacted hydroxyl groups of the BPA in the membrane. As a result, the number of OH bonds on the surface decreased by 29.8%. ii) The excess concentration of TMC in the solution led to the hydrolysis of TMC with water to form carboxylic acids. The presence of carboxylic acid group in the FTIR spectrum of the membrane PE TFNC1_20 was

confirmed by the broadening of the peak at 1720 cm^{-1} together with the appearance of a larger contribution in the range 2300–2700 cm^{-1}, and was hypothesized to be due to a mixture of 1,3,5-benzene tricarboxylic acid and 1,3-benzene dicarboxylic acid (see Figure S2-A). Both reactions led to a 71.8% increase of the CO bonding value (Figure 4A). Consequently, the membrane PE TFNC1_20 exhibited much lower OH/CO bonding ratio than the other membranes prepared with shorter IP reaction times.

3.1.2. Effects of the polymerization reaction time on the filtration performance and antifouling capacity of polyester thin film nanofiber composite membranes

Figure 5 A-B shows the HA permeate flux (J_{HA}) and the HA separation factor (α) of the unmodified supporting membrane (ENM1) and the PE TFNC membranes prepared with different polymerization times as a function of the filtration time. Compared to ENM1, J_{HA} was decreased with the increase of the IP reaction time. This reduction was quantified with the change of the mean HA permeate flux (i.e. average J_{HA} over the whole filtration test; $\overline{J_{HA}}$) (see Table 3). The value of $\overline{J_{HA}}$ decreased almost linearly with the increase of the reaction time from 5 to 15 min (i.e. 1.5 to 6 times lower) but changed sharply for 20 min (i.e. up to 36 times lower). This trend in flux reduction agrees well with the reduction of the mean size of the inter-fiber space ($\overline{d_f}$) of the membranes and the changes observed in their surface due to the film formation process (see Figure 3 A-C). A substantial reduction of the permeate flux of TFC membranes after a critical reaction time of the polymerization process was previously reported by other authors [14, 16, 27, 30]. This behaviour was generally related to a significant increase of the degree of crosslinking, which increased the thickness of the formed thin film, increasing the permeability resistance of the membrane.

The observed changes of the HA separation factor (α) of the PE TFNC membranes with the increase of the polymerization reaction time followed a different trend than that reported for the permeate flux (see Figure 5B). From 5 to 15 min IP reaction time, no significant enhancement of the separation factor was detected. The α values of the membranes PE TFNC1_5, PE TFNC1_10 and PE TFNC1_15 were very similar to that of the ENM 1 support and the mean value of the HA separation factor ($\bar{\alpha}$ in Table 3) was increased by only 8.4, 7.7 and 8.1%, respectively. These membranes were not fully covered by the PE thin film. However, a noticeable enhancement (57.6%) was observed for the $\bar{\alpha}$ value of the membrane PE TFNC1_20 compared to ENM1 due to the fact that the membrane PE TFNC1_20 was entirely covered with the PE layer, which strongly decreased its $\overline{d_f}$ value. This phenomenon was also reported previously by other researchers who developed TFC membranes using different monomers and supports [6, 9, 27]. For instance, a significant increase in rejection of $MgSO_4$ (from 21.2 to 83.9%) was also observed by Zhang et al. [6] when a sharply decrease in the water permeability (from 15.1 to 6.0 L/m^{2}h.bar) of polyesteramide (PEA) TFC membranes occurred at prolonged IP reaction time.

It is worth noting that the filtration performance index (*PI*) of the membranes (Table 3) decreased with increasing the IP reaction time following the same trend as the final HA permeate flux (J_{HA_f}) (Table 3). This highlights the predominant effect of the J_{HA_f} on the *PI* of the membrane over its final separation factor (α_f) . For instance, despite the considerable enhancement of α_f of the membrane PE TFNC1_20, its *PI* decreased 73.6% with respect to the membrane PE TFNC1_15 due mainly to the strong reduction of its permeate flux.

The antifouling properties of the membranes were evaluated by determining their irreversible fouling factor (FR_W) after the HA filtration tests as described earlier. The

results are summarized in Table 3 and plotted in Figure 5C. All surface modified PE TFNC membranes exhibited lower fouling tendency than that of the ENM1 support. Compared to this membrane (FR_W = 96.8%), the FR_W value of the PE TFNC membranes decreased with the IP reaction time to 10.2% for the membrane PE TFNC1_15 (i.e. ~90% of the initial water permeate flux (J_{w_0}) was recovered after cleaning the membrane with pure water). An increase of the FR_W value was detected when further increasing the IP reaction time to 20 min (22.9%), but it remained smaller than that of the membranes PE TFNC1_5 (93.3%) and PE TFNC1_10 (52.6%). Photographs of the ENM1 support and the PE TFNC membranes after performing the HA filtration tests (Figure 5D) are consistent with the mentioned FR_W results. The membrane with the best antifouling performance (PE TFNC1_15) showed the lowest HA deposition on its surface.

The trend of the fouling tendency with IP reaction time can be explained by the changes in the morphological structure of the PE TFNC membranes (Table 3). It is well known that membrane surface roughness, hydrophilicity and charge density are the three major factors affecting fouling phenomena [3-6]. Foulants preferentially accumulate and adhere to a hydrophobic and rough membrane surface while those deposited on a hydrophilic and smooth surface are easily removed [5]. The PE layer formed during the first 15 min of the IP process made the surface of the membrane less rough (Figure 3A), which therefore reduced its fouling tendency (i.e. FR_W value was reduced from 96.8 to 10.2%). With a further increase of the IP reaction time to 20 min, the membrane surface became rougher than that obtained for 15 min and the FR_W value was increased ($FR_{W,\ 20\ \mathrm{min}}$ = 22.9%, see Table 3). Seman et al. [45] also found a clear correlation between the roughness of BPA PE TFC membranes and the obtained FR_W values.

Additionally, the unreacted residual hydroxyl groups (–OH) on the membrane surface can effectively enhance the membrane hydrophilicity and therefore its antifouling capacity against hydrophobic foulants [3, 5, 6]. The increasing number of the OH groups on the membrane surface with the increase of the IP reaction time from 5 to 15 min (Figure 4B) agrees well with the reduction of the FR_W of the corresponding PE TFNC membranes. For 20 min reaction time, the membrane PE TFNC1_20 exhibited a reduced OH bonding, which together with its rougher surface decreased its fouling resistance compared to the membrane PE TFNC1_15.

The electrostatic interaction between the membrane surface and solutes in the feed solution also affects particles deposition and fouling tendency [6, 29]. At pH 11, both HA particles and PSU ENMs are negatively charged [37]. According to the values of the ζ-potential shown in Table 3, all PE TFNC membranes exhibited higher negative surface charge (i.e. lower ζ-potential values) than that of the ENM1 support. Therefore, the electrostatic repulsion between the HA particles and the membrane surface increased, resulting in a lower HA fouling tendency. The increase of the negative surface charge was caused by the presence of the –OH and –COOH groups on the membrane surface, or which is the same by the phenoxide and carboxylate ions ($–O^-$, $–COO^-$) at a basic pH [5, 18]. The membrane PE TFNC1_15 had the lowest ζ-potential value

(-72.5 mV) and the lowest FR_W value (10.2%) as well indicating its greatest antifouling performance.

(**Insert references Table 5: [3-8, 10, 29, 32-34, 50, 53, 54]**)

Taking into account the results of both the filtration and the antifouling performance of all PE TFNC membranes, the membrane PE TFNC1_15 was selected as the best membrane and therefore, 15 min was considered as the optimum IP reaction time to

prepare these PE TFNC membranes. Compared to other reported PE TFC membranes [7, 8, 29, 32, 50, 53] (see Table 5), the optimized PE TFNC1_15 exhibited very good filtration performance, with an extremely high water permeability (213.0 L/m^{2}h.bar at 23°C, up to 2 orders of magnitude higher) and a competitive final HA separation (72.5%). For instance, the PE TFC membrane developed by Cheng et al. [32] with a similar optimum IP reaction time (20 min) and a comparable negative surface charge (ζ-potential = -57.4 mV) to that of the membrane PE TFNC1_15, exhibited a much lower water permeability (1.34 L/m^{2}h.bar at 25°C) and only a $MgSO_4$ rejection of 67.9%. In terms of antifouling performance, the optimized membrane PE TFNC1_15 in the present study exhibited a FR_W value as low as 10.2%, comparable to that of the PE TFC membrane prepared by Seman et al. [7] (FR_W = 5%) used also for the treatment of 15 mg/L HA solutions under basic conditions.

3.2. Polyester thin film composite membranes prepared with different supports

The effects of the supporting membrane on the formation of the PE thin film layer and on the physicochemical and filtration properties of PE TFC membranes were investigated.

A second heat-treated optimized PSU ENM (ENM2) and a commercial PES MF membrane (PES) were used as supports to prepare PE TFC membranes following the same IP procedure to get the best PE TFNC membrane in the previous section (PE TFNC1_15: 2% w/v BPA reacts with 0.25% w/v TMC for 15 min IP reaction time). The morphological properties and *PWP* values of all different supporting membranes are summarized in Table 1. Although the morphological properties of the three selected supports (ENM1, ENM2, PES) are different, their filtration performance under the same conditions are high as reported in our previous study [36].

3.2.1. Effect of the supporting membrane on the physicochemical properties of polyester thin film composite membranes

The physicochemical properties of the supporting membranes and the corresponding PE TFC membranes are displayed in Figure 6. The observed differences between the surface morphology of the PE TFC membranes (Figure 6A) suggested that the supporting membrane affected the formation of the PE film layer. While the membrane PE TFNC1_15 exhibited a smooth surface, the membranes PE TFNC2_15 and PE TFC_15 had rougher surfaces with nodular structure similar to that of the membrane PE TFNC1_20 (Figure 3A). Compared to their supports, a clear reduction of the mean pore size ($\overline{d_f}$) of all surface modified membranes was observed. The $\overline{d_f}$ values decreased by 30.0, 51.6 and 19.3% for the membranes PE TFNC1_15, PE TFNC2_15 and PE TFC_15, respectively (see Figure 6 B-C and data in Table 3).

It worth quoting that during IP, the hydrophilicity and the pore size of a supporting membrane are key parameters affecting film formation [20, 21, 23, 24, 35]. For instance, Singh et al. [20] studied the structural variations of PA TFC membranes prepared over PSU porous membranes with different pore sizes. It was reported that a two-fold thicker PA thin film layer was formed on the supporting membrane with a smaller pore size. Kaur et al. [35], who studied the influence of the nanofiber diameter ($\overline{\lambda_w}$) of ENMs supports on the formation of the PA thin film layer, claimed that the ENMs with larger $\overline{\lambda_w}$ resulted in a thinner PA layer with a smoother structure, whereas when the value of $\overline{\lambda_w}$ was smaller, the packing density of the nanofibers was higher and the inter-fiber space was lower, favouring a rougher PA layer with a more cross-linked and packed structure. Ghosh and Hoek [21] investigated the influence of the physical and chemical properties of different porous PSU supports on the PA thin film layer characteristics. More hydrophobic supports resulted in a thicker and rougher PA thin

film layer. The above mentioned results agree well with the different morphological structures of the membranes PE TFNC1_15 and PE TFNC2_15 (Figure 6A). The ENM2 support had a smaller inter-fiber space and nanofiber diameters, and a higher water contact angle (i.e. more hydrophobic) than ENM1 (Table 1). Therefore, a thicker and rougher PE layer was expected for the membrane PE TFNC2_15 compared to the membrane PE TFNC1_15. After IP, the reduction of the $\overline{d_f}$ value of the membrane PE TFNC2_15 was almost 2 times higher than that of the membrane PE TFNC1_15. In addition, the membrane PE TFC_15 had a rougher surface than the membrane PE TFNC1_15, which was also consistent with the results reported in previous studies as the PES support had 5.6 times smaller $\overline{d_f}$ value than ENM1 [21].

FTIR spectra of the unmodified supporting membranes together with their respective surface modified membranes are displayed in Figure 6D. An excess of BPA was detected in all surface modified membranes, as their FTIR spectra showed a weak adsorption peak at about 1612 cm^{-1} and a larger contribution of the peaks at 1509 and 832 cm^{-1} compared to the FTIR spectra of their supports, mainly attributed to the C=C aromatic stretching vibration of the ring of the BPA moiety. However, the BPA excess in the membranes PE TFNC2_15 and PE TFC_15 was lower than that of the membrane PE TFNC1_15, as the respective intensities of the peaks were lower than those observed in the FTIR spectrum of the membrane PE TFNC1_15. New absorption peaks of the ester group bands at 1720 and 1200 cm^{-1} were observed for all surface modified membranes confirming the successful formation of the PE thin film layer regardless of the supporting membrane used. The peak assigned to the C=O stretching vibration of the ester group at 1720 cm^{-1} of the membranes PE TFNC2_15 and PE TFC_15 was much wider than that of the membrane PE TFNC1_15, mainly due to a new contribution centered at 1698 cm^{-1}, which revealed the presence of carboxylic acid

groups (–COOH). These –COOH groups for the membranes PE TFNC2_15 and PE TFC_15 were responsible for the shift of the center of the broad absorption peak between 3150–3700 cm^{-1} (stretching vibration of the hydroxyl groups (–OH) of the membranes) to higher wavenumbers (~3393 cm^{-1}) compared to that of the membrane PE TFNC1_15 (~3355 cm^{-1}) (Figure S2-B). In addition, similar to the FTIR spectrum of the membrane PE TFNC1_20, a broad contribution between 2300 and 2700 cm^{-1} and a narrow peak at 3110 cm^{-1} also emerged in the FTIR spectra of the membranes PE TFNC2_15 and PE TFC_15 due to the presence of –COOH groups (Figure S2 A-B). The chemical structural differences in the FTIR spectra of the membranes PE TFNC2_15 and PE TFC_15 compared to that of the membrane PE TFNC1_15 agreed with the morphological structural differences observed in the SEM surface images of their formed PE thin film layers (Figure 6A). As it was explained in section 3.1.1, the surface modified membrane having carboxylic acid groups (PE TFNC1_20) reached a higher degree of crosslinking during IP, resulting in a denser, thicker and rougher PE film layer. Based on the similarities between the surface morphology and the FTIR spectra of the membranes PE TFNC2_15 and PE TFC_15 (Figure 6A and 6D) and that of the membrane PE TFNC1_20 (Figure 3A and 3D), it could be deduced that the smaller pore size of the ENM2 and PES supports favoured a faster IP reaction compared to ENM1 and resulted in the formation of a thick and rough PE layer with high crosslinking degree in only 15 min IP reaction time.

3.2.2. Effect of the supporting membrane on the filtration performance of polyester thin film composite membranes

All surface modified membranes exhibited lower J_{HA} and greater α values than those of their respective supports (Figure 7 A-B). The reduction of the permeate flux was expected because of the reduction of the mean pore size ($\overline{d_f}$) of the PE TFC membranes

and the subsequent increase of the permeate resistance due to the formation of the PE layer. The greatest reduction of $\overline{J_{HA}}$ was observed for the membrane PE TFNC2_15 (97%), which also experienced the greatest reduction of its $\overline{d_f}$ compared to its support. In general, it is expected a decline of J_{HA} with the filtration time due mainly to fouling phenomena. However, J_{HA} of the membrane PE TFC_15 increased with time. Its water permeate flux after conducting HA filtration test was 3.2 times higher than its initial water permeate flux. This unexpected behavior may be due to the partial detachment of the PE layer from the PES support during HA filtration test, decreasing the permeate resistance of the membrane. Bui et al. [49] also found adhesion problems of the PA layer to the PES support when developing PA TFNC membranes on PSU ENMs and PES ENMs. Compared to PSU ENM support, a weaker adhesion of the PA layer to the PES ENM support was observed so that delamination and, in some cases, detachment of the PA layer from the PES support occurred. It was hypothesized that the BPA moiety difference between the chemical composition of PSU and PES together with the higher water contact angle of the PSU support contributed to the good adhesion of the PA layer to PSU. In the present study, the PES support exhibited up to 4.7 times lower water contact angle value than the PSU ENM1 and ENM2 supports, which basically may reduce the adhesion capability of PE layer to PES support. Moreover, taking into consideration that ENM1 and ENM2 are electrospun nanofibrous PSU supports with inter-fiber spaces bigger than the pore size of the PES phase inversion membrane support, the BPA in the aqueous phase may penetrate easily through part of the nanofiber network favoring the formation and growth of the PE layer from the inter-fiber space and resulting in a better adhesion.

The enhancement of α for all surface modified membranes compared to their corresponding supports (Figure 7B) was mainly related to the formation of the PE layer

and reduction of their $\overline{d_f}$. In addition, the surface modified membranes exhibited lower ζ-potential values (i.e. higher negative surface charge, see Table 3) than their supports, which resulted in an enhancement of the electrostatic repulsion forces between the HA particles and the membrane surface favouring the HA separation as consequence.

All surface modified membranes exhibited better antifouling capacity (i.e. lower FR_W values, Table 3) than their respective supports. The negative FR_W value determined for the membrane PE TFC_15 resulted from the increase of the water permeate flux from its initial value after the HA filtration test. The FR_W value of the membrane PE TFNC2_15 (20.1%) was larger than that of the membrane PE TFNC1_15 (10.2%). Both membranes exhibited quite similar ζ-potential values (Table 3), but the membrane PE TFNC2_15 had a rougher PE layer, which contributed to its higher fouling tendency (higher FR_W value).

The photographs shown in Figure 7D of the unmodified and surface modified membranes after HA filtration tests are consistent with the mentioned results of the FR_W. The surface of the membrane PE TFNC1_15 with the lowest HA deposition is the membrane with the best antifouling performance (i.e. lowest FR_W value). It is to be noted that although the FR_W value calculated for the membrane PE TFC_15 was negative, HA was deposited on its entire surface indicating that this membrane also experienced fouling.

The filtration performance of the different membranes used as supports as well as the surface modified membranes were evaluated using their *PI* values (see Figure 7C and Table 3). The membrane PE TFNC2_15 exhibited the lowest *PI* value (26.6 kg/m^2 h), whereas membranes PE TFNC1_15 and PE TFC_15 achieved similar *PI* values (70.4 and 68.7 kg/m^2 h, respectively). Although the membranes PE TFNC1_15 and PE TFC_15 exhibited similar *PI* values, their physicochemical and morphological

properties together with other filtration parameters were different. For instance, the initial water permeate flux (J_{w_0}) of the membrane PE TFNC1_15 (213 kg/m^2 h) was 8 times higher than that of the membrane PE TFC_15 (26 kg/m^2 h). The HA filtration test showed that the $\overline{J_{HA}}$ value of the membrane PE TFNC1_15 (151 kg/m^2 h) was 3 times higher than that of the membrane PE TFC_15 (51 kg/m^2 h), but its HA separation factor (α_f = 72.5%) was worse than that of the membrane PE TFC_15 (α_f = 86.9%). In addition, from the photographs of the membranes taken after HA filtration tests (Figure 7D), less HA deposition was observed on the surface of the membrane PE TFNC1_15 compared to that of the membrane PE TFC_15. Taking into account both the filtration performance and antifouling capacity of these membranes and considering the lack of stability of the PE thin layer of the membrane PE TFC_15 (i.e. detachment due to poor adhesion of PE to its support), the membrane PE TFNC1_15 was chosen as the best PE TFC membrane developed in this study.

3.3. Polyester *versus* polyamide thin film composite membranes

It is worth quoting that most TFC membranes have been prepared with IP that involved amine monomers in the aqueous phase to form a PA thin film layer on a supporting membrane. Compared to PA TFC membranes, very few research studies have been focused on PE TFC membranes. This may be due to the greater salt rejection of the PA TFC membranes compared to that of PE TFC membranes attributed to their denser structure with a high crosslinking degree although the PE TFC membranes exhibited better antifouling capacity against hydrophobic contaminants because of the presence of abundant hydroxyl groups on their surface [5, 6]. In this section, PA TFC membranes were prepared and their filtration and antifouling properties were compared to those of the previously prepared PE TFC membranes that exhibited a high filtration performance (PE TFNC1_15 and PE TFC_15 in Table 3).

Different combinations of monomers and conditions of the IP process were considered to form the PA thin film layer. Details of the followed procedure to select the final IP approach can be found in the SI (see Figures S3-S9 and Tables S1-S4). The selected IP consists of 1% w/w PIP that reacted with 2% w/v TMC in presence of 1% w/w TEA (acid acceptor) during 5 min IP reaction time. The schematic mechanism of this IP reaction is shown in Figure 2B. Both ENM1 and the MF commercial PES membrane were used as supports to form the membranes PA TFNC1_5 and PA TFC_5, respectively.

3.3.1. Physicochemical properties of polyamide thin film composite membranes

The structure of the PA TFC membranes (PA TFNC1_5 and PA TFC_5) was studied by means of SEM (Figure 8A). The surface morphology of these membranes were different from the corresponding PE TFC membranes (PE TFNC1_15 and PE TFC_15). The PA thin film layer of the membrane PA TFNC1_5 was formed in the inter-fiber space wrapping the PSU nanofibers and preserving the nanofiber structure of the support and its roughness (see also Figure S10). A similar surface morphology of PA TFNC membranes was observed by other authors [35, 49]. The membrane PA TFC_5 showed a rough PA layer that covered completely the surface of the PES support. The granular structure formed throughout the PA layer of both membranes is typically attributed to the crosslinking of the used monomers PIP and TMC [16, 18, 55]. From the SEM images, the thin film layer of the membrane PA TFC_5 seemed to be denser than that of the membrane PA TFNC1_5. The porometry measurements confirmed the reduction of the $\overline{d_f}$ value of the membranes PA TFNC1_5 and PA TFC_5 with respect to their supports due to the addition of the PA layer (Figure 8 B-C and Table 3).

The differences in the chemical structure of the PA TFC membranes were studied by FTIR spectra shown in Figure 8D. Table 4 summarizes the assignments of IR bands for

682 the ENM1 and PES supports as well as for the PA TFC membranes. Beside the typical
683 IR bands of the PSU and PES substrates, the spectra of the PA TFC membranes
684 exhibited absorption peaks at about 1442 and 1616 cm^{-1}. The peak at 1442 cm^{-1} was
685 assigned to the C-O stretching and the O-H bending vibration of the carboxylic acid
686 group as well as to the bending vibration of the methylene group (-CH_2-). Whereas the
687 peak at 1616 cm^{-1} was attributed to the C=O and the C-N stretching vibrations of the
688 amide bond formation (–CONH) (amide I band). Furthermore, the broad adsorption
689 peak between 3150–3700 cm^{-1} centred at about 3426 cm^{-1} for the membrane PA
690 TFNC1_5 and at 3393 cm^{-1} for the membrane PA TFC_5 was mainly attributed to the
691 O-H stretching vibration of the carboxylic acid group (–COOH) formed by the partial
692 hydrolysis of the acyl chloride unit of TMC. It was reported that some contribution to
693 the latter peak could also correspond to the N-H stretching vibration of residual amine
694 bonds [6, 13, 48]. The membrane PA TFC_5 also displayed a peak at 1283 cm^{-1}, which
695 could be assigned to the N-H in-plane bending coupled with the C-N stretching or to
696 the C- H and N- H deformation vibration of amide III band. The membrane PA
697 TFNC1_5 exhibited a peak at about 1697 cm^{-1} attributed to the C=O stretching
698 vibration of the carboxylic acid group. The presence of all the above cited peaks
699 verified the successful formation of the PA thin layer on the surface of both supports,
700 ENM1 and PES. The intensity of the peak at about 1616 cm^{-1} (previously ascribed to
701 the amide bond formation) was higher for the membrane PA TFC_5 compared to the
702 membrane PA TFNC1_5, indicating a thicker, denser and more cross-linked PA thin
703 layer of the membrane PA TFC_5. This result was also confirmed by the characteristic
704 IR bands of the PES support that were much more attenuated (some peaks even
705 disappeared) in the FTIR spectrum of the membrane PA TFC_5 than those of the PSU
706 support in the FTIR spectrum of the membrane PA TFNC1_5. These results agree well

with those reported by Singh et al. [20], who claimed the formation of a thicker PA thin film layer over a supporting membrane with smaller pore sizes.

3.3.2. Comparison of the filtration performance of polyester and polyamide thin film composite membranes

The filtration performance of the PA TFC membranes (PA TFNC1_5, PA TFC_5) was evaluated and compared with that of the previously prepared PE TFC membranes (PE TFNC1_15, PE TFC_15) and the corresponding supporting membranes (ENM1, PES).

The change of the HA permeate flux (J_{HA}) and the HA separation factor (α) with the filtration time were plotted in Figure 9 A-B. The membrane PA TFNC1_5 exhibited lower J_{HA} than that of the ENM1 support. The value of $\overline{J_{HA}}$ decreased by 68.9% compared to that of the ENM1 (from 929.5 to 289.1 kg/m^2 h). This reduction of the permeate flux was mainly attributed to the reduction of the $\overline{d_f}$ value of the modified membrane. However, unlike the other surface modified TFC membranes developed in this study, the α value of the membrane PA TFNC1_5 decreased (by 6.9%) in relation to ENM1 instead of increasing. Not only the pore size of the membrane (i.e. stereo-hindrance or sieving effect) affects its separation capacity, but also the electrostatic interaction between the HA molecules and the membrane surface (i.e. electrostatic repulsion effect). After IP modification, the membrane PA TFNC1_5 exhibited a higher ζ-potential value (-49.2 mV) compared to ENM1 (-59.4 mV). The lower negative surface charge of the membrane PA TFNC1_5 resulted in a reduction of the electrostatic repulsion between the HA molecules and the membrane surface. In this case, both the electrostatic repulsion and size exclusion reduced the HA separation factor of the membrane PA TFNC1_5.

Despite its lower negative surface charge (i.e. a higher ζ-potential value), the membrane PA TFNC1_5 showed a better antifouling performance (FR_W = 46.4%) than that of the ENM1 (FR_W = 96.8%). As stated previously, the antifouling properties of the membranes depend mainly on the roughness, charge density and hydrophilicity of the membrane surface. After IP modification, the surface of the membrane PA TFNC1_5 contained carboxylic acid group and amine end groups, which improved its hydrophilicity compared to ENM1 [5, 16, 55]. This could be the reason of the improved antifouling properties of the membrane PA TFNC1_5. The photographs of the membranes PA TFNC1_5 and ENM1 after HA filtration tests shown in Figure 9D are consistent with the better antifouling performance of the membrane PA TFNC1_5 because less HA was deposited on its surface.

A significant decrease of J_{HA} was observed for the membrane PA TFC_5 compared to the PES support, leading to a reduction of its $\overline{J_{HA}}$ value by 97.9%. In addition, surface modification improved the separation capacity of the membrane PA TFC_5 in relation to PES by 24.3% from $\bar{\alpha}$ = 56.4% to $\bar{\alpha}$ = 70.1%. The strong decrease of the permeate flux together with the increase of the separation factor of the membrane PA TFC_5 was attributed mainly to the reduction of the $\overline{d_f}$ of the membrane due to the highly cross-linked PA layer formed on its surface. The membrane PA TFC_5 displayed also a lower negative surface charge (ζ-potential = -34.8 mV) than PES (ζ-potential = -46.4 mV), but the combining effect of the electrostatic repulsion and the size exclusion together with the high density of the PA layer improved the HA separation of the membrane PA TFC_5. The antifouling performance of the membrane PA TFC_5 was also improved compared to that of its support as it can be seen from Figure 9D where much less HA was deposited on its surface after filtration. The reduction of the fouling tendency of the membrane PA TFC_5 was likely due to the enhancement of its surface hydrophilicity

after IP modification. An increase of J_{HA} with the filtration time was also observed for the membrane PA TFC_5 and its final water permeate flux after HA filtration test was larger than its initial water flux. As a result, the membrane PA TFC_5 exhibited a negative FR_W value (see Table 3). Similar to the membrane PE TFC_15 (section 3.2.2), this phenomenon could be explained by the partial detachment of the PA thin layer during the HA filtration test, which reduced the permeate resistance of the membrane.

A 74-fold higher *PWP* value was achieved by the membrane PA TFNC1_5 (i.e. 324 L/m^{2}h.bar) compared to the membrane PA TFC_5 (i.e. 4.4 L/m^{2}h.bar) (Table 3). The higher permeate flux of the membrane PA TFNC1_5 was likely due to the interconnected nanofibrous structure of the ENM1 support having a higher porosity than the PES support and to the formation of water channels through the interface between the nanofibers and the PA thin layer of the membrane PA TFNC1_5 [33].

From the HA tests, the reduction of $\overline{J_{HA}}$ for the membrane PA TFC_5 compared to its support (97.9%) was higher than that of the membrane PA TFNC1_5 (68.9%). This is consistent with the previously mentioned chemical and structural differences of these membranes. The thicker, denser and more cross-linked PA thin layer of the membrane PA TFC_5 caused a higher reduction of the permeate fluxes and an improved HA separation performance. Moreover, the increase of the ζ-potential of this membrane from that of its support (25.0%) was also greater than that of the PA TFNC1_5 (17.2%). This justified the more cross-linked PA thin film layer of the membrane PA TFC_5. It is well known that the negative surface charge of this type of poly(piperazine-amide) TFC membranes is mainly attributed to the deprotonation of carboxyl groups (–COOH → –COO$^-$) dissociated from the unreacted acid chlorides of TMC [10, 18]. Therefore, the greater crosslinking degree of the PA layer of the membrane PA TFC_5 indicated the lower amount of carboxyl groups available to be deprotonated and the subsequent lower

781 negative surface charge of the membrane PA TFC_5 compared to that of the membrane
782 PA TFNC1_5 [18].

783 The data summarized in Table 5 for different reported PE and PA TFC membranes
784 showed the good filtration performance of the prepared PA TFC membranes in this
785 study. For instance, the permeability of the membrane PA TFNC1_5 was up to two
786 orders of magnitude higher than that of lab-made PA TFNC membranes prepared with
787 similar IP conditions [33, 34], whereas its separation factor was 21 to 30% lower. The
788 membrane PA TFC_5 exhibited a very similar separation factor (only 1.5% higher α_f
789 value) than that of the lab-made PA TFC membranes with 7 to 32% higher permeability
790 [4, 5].

791 Regardless of the type of polymer of the thin film layer (i.e. PE or PA), all surface
792 modified membranes exhibited lower fouling tendency (i.e. FR_W values from 10.2 to
793 93.3%, see Table 3) than their supports (i.e. FR_W values from 96.8 to 98.5%) than their
794 supports.

795 All surface modified membranes prepared on ENM1 support (PE TFNC1_15, PA
796 TFNC1_5) exhibited greater *PI* values (70.4 and 87.4 kg/m^2 h, respectively) than those
797 prepared on PES support (68.7 kg/m^2 h for PE TFC_15 and 5.8 kg/m^2 h for PA TFC_5)
798 (see Figure 9C and Table 3). The improved *PI* values of the TFNC membranes resulted
799 mainly from their much larger permeability, which is directly related to the
800 interconnected open pore structure and the high porosity of the nanofiber support.

801 In order to select the best membrane between PE TFNC1_15 and PA TFNC1_5,
802 both the filtration and antifouling performance should be considered. The *PI* of the
803 membrane PE TFNC1_15 (70.4 kg/m^2 h) was 20% lower than that of the membrane PA
804 TFNC1_5 (87.4 kg/m^2 h). This was caused mainly by its lower J_{HA_f} value, 97.1 kg/m^2 h,
805 compared to 126.7 kg/m^2 h of the membrane PA TFNC1_5 although its HA separation

806 factor was higher (72.5%) than that of the membrane PA TFNC1_5 (69.0%). In
807 addition, the membrane PE TFNC1_15 had better antifouling performance, exhibiting a
808 4.5 times lower FR_W value (10.2%) than that of the membrane PA TFNC1_5 (46.4%).
809 Due to its enhanced antifouling properties, the water permeability of the membrane PE
810 TFNC1_15 after HA filtration test was larger (i.e. 191.3 kg/m^2 h bar) than that of the
811 membrane PA TFNC1_5 (i.e. 173.7 kg/m^2 h bar). The lower fouling tendency of the
812 membrane PE TFNC1_15 guarantees it a longer lifetime and reduces maintenance costs.
813 Taking into account all the above mentioned points, the membrane PE TFNC1_15 was
814 chosen as the best TFC membrane developed in this study. This membrane exhibited
815 comparable antifouling performance to previously reported PE TFC membranes with
816 two orders of magnitude greater water permeability [29] and 6–33% better separation
817 factor [32, 50]. Compared to other PA TFC membranes, it exhibited 34–83% greater
818 antifouling performance [5, 10] and 10–71 times higher water permeability [5, 34] with
819 only 17–27% lower separation efficiency [33, 34] (Table 5).

820 **4. Conclusions**

821 The effects of the polymerization reaction time on the physicochemical, filtration and
822 antifouling characteristics of the PE TFNC membranes were studied. The optimum IP
823 reaction time was found to be 15 min. The so prepared membrane PE TFNC1_15 had a
824 smooth surface and exhibited a water permeability as high as 213.0 L/m^{2}h.bar with a
825 72.5% HA separation factor. The enhanced antifouling performance of this membrane
826 against HA foulant permitted 90% recovery of its initial water flux after HA filtration.

827 The surface of the PE layer formed on the ENM2 supporting membrane with a
828 smaller mean size of the inter-fiber space and a higher hydrophobicity was rougher and
829 denser than that prepared on ENM1. The PE layer prepared on the commercial PES
830 supporting membrane had a very similar surface morphology to that formed on ENM2.

The PE TFC membranes formed on ENM2 and PES supports (i.e. PE TFNC2_15 and PE TFC_15, respectively) exhibited lower filtration performance indexes and worse antifouling properties than that of the PE TFC membrane prepared on ENM1 (i.e. PE TFNC1_15).

The PA layer formed on PES support was denser and higher cross-linked than that prepared on ENM1. Regardless of the type of polymer of the thin layer, PE or PA, all surface modified TFC membranes prepared on ENM1 support (PE TFNC1_15, PA TFNC1_5) exhibited greater filtration performance indexes than that of the TFC membranes prepared on PES support (PE TFC_15, PA TFC_5). The membrane PE TFNC1_15, prepared with 15 min IP reaction time of BPA and TMC on ENM1, was chosen as the best TFC membrane developed in this study as it exhibited the best antifouling capacity with a high filtration performance.

Acknowledgments

The authors gratefully acknowledge the financial support of the Spanish Ministry of Economy and Competitiveness through its project CTM2015-65348-C2-2-R and the Spanish Ministry of Science, Innovation and Universities through its project RTI2018-096042-B-C22. The authors thank José Emilio Fernández Rubio PhD, Center of Infrared and Correlation Spectroscopy, for his valuable comments on FTIR spectra analysis. P. Arribas also thanks the Campus of International Excellence, Moncloa Campus (UCM-UPM), for the PhD grant.

Supplementary data

Supplementary Information (SI) is available.

References

[1] S. Zinadini, S. Rostami, V. Vatanpour, E. Jalilian, Preparation of antibiofouling polyethersulfone mixed matrix NF membrane using photocatalytic activity of ZnO/MWCNTs nanocomposite, J. Membr. Sci., 529 (2017) 133-141.

[2] Y. Mo, A. Tiraferri, N.Y. Yip, A. Adout, X. Huang, M. Elimelech, Improved antifouling properties of polyamide nanofiltration membranes by reducing the density of surface carboxyl groups, Environ. Sci. Technol., 46 (2012) 13253-13261.

[3] F. Yan, H. Chen, Y. Lü, Z. Lü, S. Yu, M. Liu, C. Gao, Improving the water permeability and antifouling property of thin-film composite polyamide nanofiltration membrane by modifying the active layer with triethanolamine, J. Membr. Sci., 513 (2016) 108-116.

[4] H. Li, W. Shi, Q. Du, R. Zhou, H. Zhang, X. Qin, Improved separation and antifouling properties of thin-film composite nanofiltration membrane by the incorporation of cGO, Applied Surface Science, 407 (2017) 260-275.

[5] J. Rezania, V. Vatanpour, A. Shockravi, M. Ehsani, Preparation of novel carboxylated thin-film composite polyamide-polyester nanofiltration membranes with enhanced antifouling property and water flux, Reactive and Functional Polymers, 131 (2018) 123-133.

[6] R. Zhang, S. Yu, W. Shi, W. Wang, X. Wang, Z. Zhang, L. Li, B. Zhang, X. Bao, A novel polyesteramide thin film composite nanofiltration membrane prepared by interfacial polymerization of serinol and trimesoyl chloride (TMC) catalyzed by 4□dimethylaminopyridine (DMAP), J. Membr. Sci., 542 (2017) 68-80.

[7] M.N. Abu Seman, M. Khayet, N. Hilal, Development of antifouling properties and performance of nanofiltration membranes modified by interfacial polymerisation, Desalination, 273 (2011) 36-47.

[8] Y. Zhang, Y. Su, J. Peng, X. Zhao, J. Liu, J. Zhao, Z. Jiang, Composite nanofiltration membranes prepared by interfacial polymerization with natural material tannic acid and trimesoyl chloride, J. Membr. Sci., 429 (2013) 235-242.

[9] C. Zhou, Y. Shi, C. Sun, S. Yu, M. Liu, C. Gao, Thin-film composite membranes formed by interfacial polymerization with natural material sericin and trimesoyl chloride for nanofiltration, J. Membr. Sci., 471 (2014) 381-391.

[10] A. Akbari, E. Aliyarizadeh, S.M. Mojallali Rostami, M. Homayoonfal, Novel sulfonated polyamide thin-film composite nanofiltration membranes with improved water flux and anti-fouling properties, Desalination, 377 (2016) 11-22.

[11] N.K. Saha, S.V. Joshi, Performance evaluation of thin film composite polyamide nanofiltration membrane with variation in monomer type, J. Membr. Sci., 342 (2009) 60-69.

[12] J. Xiang, Z. Xie, M. Hoang, K. Zhang, Effect of amine salt surfactants on the performance of thin film composite poly(piperazine-amide) nanofiltration membranes, Desalination, 315 (2013) 156-163.

[13] Y. Li, Y. Su, Y. Dong, X. Zhao, Z. Jiang, R. Zhang, J. Zhao, Separation performance of thin-film composite nanofiltration membrane through interfacial polymerization using different amine monomers, Desalination, 333 (2014) 59-65.

[14] C. Klaysom, S. Hermans, A. Gahlaut, S. Van Craenenbroeck, I.F.J. Vankelecom, Polyamide/Polyacrylonitrile (PA/PAN) thin film composite osmosis membranes: Film optimization, characterization and performance evaluation, J. Membr. Sci., 445 (2013) 25-33.

[15] J. Xu, H. Yan, Y. Zhang, G. Pan, Y. Liu, The morphology of fully-aromatic polyamide separation layer and its relationship with separation performance of TFC membranes, J. Membr. Sci., 541 (2017) 174-188.

[16] N. Misdan, W.J. Lau, A.F. Ismail, Physicochemical characteristics of poly(piperazine-amide) TFC nanofiltration membrane prepared at various reaction times and its relation to the performance, Journal of Polymer Engineering, 35 (2015) 71-78.

[17] A.L. Ahmad, B.S. Ooi, Properties–performance of thin film composites membrane: study on trimesoyl chloride content and polymerization time, J. Membr. Sci., 255 (2005) 67-77.

[18] Y. Li, Y. Su, J. Li, X. Zhao, R. Zhang, X. Fan, J. Zhu, Y. Ma, Y. Liu, Z. Jiang, Preparation of thin film composite nanofiltration membrane with improved structural stability through the mediation of polydopamine, J. Membr. Sci., 476 (2015) 10-19.
[19] Z. Tang, C. Qiu, J.R. McCutcheon, K. Yoon, H. Ma, D. Fang, E. Lee, C. Kopp, B.S. Hsiao, B. Chu, Design and fabrication of electrospun polyethersulfone nanofibrous scaffold for high-flux nanofiltration membranes, Journal of Polymer Science Part B: Polymer Physics, 47 (2009) 2288-2300.
[20] P.S. Singh, S.V. Joshi, J.J. Trivedi, C.V. Devmurari, A.P. Rao, P.K. Ghosh, Probing the structural variations of thin film composite RO membranes obtained by coating polyamide over polysulfone membranes of different pore dimensions, J. Membr. Sci., 278 (2006) 19-25.
[21] A.K. Ghosh, E.M.V. Hoek, Impacts of support membrane structure and chemistry on polyamide–polysulfone interfacial composite membranes, J. Membr. Sci., 336 (2009) 140-148.
[22] K. Yoon, B.S. Hsiao, B. Chu, High flux nanofiltration membranes based on interfacially polymerized polyamide barrier layer on polyacrylonitrile nanofibrous scaffolds, J. Membr. Sci., 326 (2009) 484-492.
[23] M. Tian, C. Qiu, Y. Liao, S. Chou, R. Wang, Preparation of polyamide thin film composite forward osmosis membranes using electrospun polyvinylidene fluoride (PVDF) nanofibers as substrates, Sep. Purif. Technol., 118 (2013) 727-736.
[24] M. Fathizadeh, A. Aroujalian, A. Raisi, Effect of lag time in interfacial polymerization on polyamide composite membrane with different hydrophilic sub layers, Desalination, 284 (2012) 32-41.
[25] N. Misdan, W.J. Lau, A.F. Ismail, T. Matsuura, D. Rana, Study on the thin film composite poly(piperazine-amide) nanofiltration membrane: Impacts of physicochemical properties of substrate on interfacial polymerization formation, Desalination, 344 (2014) 198-205.
[26] L. Hu, S. Zhang, R. Han, X. Jian, Preparation and performance of novel thermally stable polyamide/PPENK composite nanofiltration membranes, Applied Surface Science, 258 (2012) 9047-9053.
[27] B.S. Ooi, J.Y. Sum, S.O. Lai, Investigation on membrane morphological and chemical properties changes at different reaction times and its effect on dye removal, Desalination and Water Treatment, 45 (2012) 250-255.
[28] A. Soroush, J. Barzin, M. Barikani, M. Fathizadeh, Interfacially polymerized polyamide thin film composite membranes: Preparation, characterization and performance evaluation, Desalination, 287 (2012) 310-316.
[29] B. Tang, Z. Huo, P. Wu, Study on a novel polyester composite nanofiltration membrane by interfacial polymerization of triethanolamine (TEOA) and trimesoyl chloride (TMC), J. Membr. Sci., 320 (2008) 198-205.
[30] X.-Z. Wei, J. Yang, G.-L. Zhang, Preparation and Characterization of Nanofiltration Membranes Synthesized by Hyperbranched Polyester and Terephthaloyl Chloride (TPC), Polymers and Polymer Composites, 20 (2012) 261-270.
[31] X.-Z. Wei, L.-P. Zhu, H.-Y. Deng, Y.-Y. Xu, B.-K. Zhu, Z.-M. Huang, New type of nanofiltration membrane based on crosslinked hyperbranched polymers, J. Membr. Sci., 323 (2008) 278-287.
[32] J. Cheng, W. Shi, L. Zhang, R. Zhang, A novel polyester composite nanofiltration membrane formed by interfacial polymerization of pentaerythritol (PE) and trimesoyl chloride (TMC), Applied Surface Science, 416 (2017) 152-159.
[33] L. Yung, H. Ma, X. Wang, K. Yoon, R. Wang, B.S. Hsiao, B. Chu, Fabrication of thin-film nanofibrous composite membranes by interfacial polymerization using ionic liquids as additives, J. Membr. Sci., 365 (2010) 52-58.
[34] S. Kaur, R. Barhate, S. Sundarrajan, T. Matsuura, S. Ramakrishna, Hot pressing of electrospun membrane composite and its influence on separation performance on thin film composite nanofiltration membrane, Desalination, 279 (2011) 201-209.

954 [35] S. Kaur, S. Sundarrajan, D. Rana, T. Matsuura, S. Ramakrishna, Influence of electrospun
955 fiber size on the separation efficiency of thin film nanofiltration composite membrane, J.
956 Membr. Sci., 392-393 (2012) 101-111.
957 [36] P. Arribas, M.C. García-Payo, M. Khayet, L. Gil, Heat-treated optimized polysulfone
958 electrospun nanofibrous membranes for high performance wastewater microfiltration, Sep.
959 Purif. Technol., (2019).
960 [37] P. Arribas, M. Khayet, M.C. García-Payo, L. Gil, Self-sustained electro-spun polysulfone
961 nano-fibrous membranes and their surface modification by interfacial polymerization for
962 micro- and ultra-filtration, Sep. Purif. Technol., 138 (2014) 118-129.
963 [38] M. Essalhi, M. Khayet, C. Cojocaru, M.C. García-Payo, P. Arribas, Response surface
964 modeling and optimization of electrospun nanofiber membranes, The Open Nanosci. J., 7
965 (2013) 8-17.
966 [39] Z. Ma, M. Kotaki, S. Ramakrishna, Surface modified nonwoven polysulphone (PSU) fiber
967 mesh by electrospinning: A novel affinity membrane, J. Membr. Sci., 272 (2006) 179-187.
968 [40] L. Li, R. Hashaikeh, H.A. Arafat, Development of eco-efficient micro-porous membranes via
969 electrospinning and annealing of poly (lactic acid), J. Membr. Sci., 436 (2013) 57-67.
970 [41] Y. Liang, S. Cheng, J. Zhao, C. Zhang, S. Sun, N. Zhou, Y. Qiu, X. Zhang, Heat treatment of
971 electrospun Polyvinylidene fluoride fibrous membrane separators for rechargeable lithium-ion
972 batteries, J. Power Sources, 240 (2013) 204-211.
973 [42] K. Smolders, A.C.M. Franken, Terminology for Membrane Distillation, Desalination, 72
974 (1989) 249-262.
975 [43] M.N.A. Seman, M. Khayet, N. Hilal, Nanofiltration thin-film composite polyester
976 polyethersulfone-based membranes prepared by interfacial polymerization, J. Membr. Sci.,
977 348 (2010) 109-116.
978 [44] Y. Mansourpanah, M. Samimi, Preparation and characterization of a low-pressure efficient
979 polyamide multi-layer membrane for water treatment and dye removal, Journal of Industrial
980 and Engineering Chemistry, 53 (2017) 93-104.
981 [45] M.N. Abu Seman, M. Khayet, N. Hilal, Development of antifouling properties and
982 performance of nanofiltration membranes by interfacial polymerization and photografting
983 techniques, in: N. Hilal, M. Khayet, C.J. Wright (Eds.) Membrane Modification: Technology and
984 Apllications, CRC Press, Taylor & Francis Group, U.S.A., 2012, pp. 119-131.
985 [46] B.R. Singh, D.B. DeOliveira, F.-N. Fu, M.P. Fuller, Fourier transform infrared analysis of
986 amide III bands of proteins for the secondary structure estimation, SPIE, 1993.
987 [47] N.-W. Oh, J. Jegal, K.-H. Lee, Preparation and characterization of nanofiltration composite
988 membranes using polyacrylonitrile (PAN). II. Preparation and characterization of polyamide
989 composite membranes, J. Appl. Polym. Sci., 80 (2001) 2729-2736.
990 [48] C.Y. Tang, Y.-N. Kwon, J.O. Leckie, Effect of membrane chemistry and coating layer on
991 physiochemical properties of thin film composite polyamide RO and NF membranes: I. FTIR
992 and XPS characterization of polyamide and coating layer chemistry, Desalination, 242 (2009)
993 149-167.
994 [49] N.-N. Bui, M.L. Lind, E.M.V. Hoek, J.R. McCutcheon, Electrospun nanofiber supported thin
995 film composite membranes for engineered osmosis, J. Membr. Sci., 385-386 (2011) 10-19.
996 [50] X. Wei, X. Kong, J. Yang, G. Zhang, J. Chen, J. Wang, Structure influence of hyperbranched
997 polyester on structure and properties of synthesized nanofiltration membranes, J. Membr. Sci.,
998 440 (2013) 67-76.
999 [51] S.G. Sanadhya, S. Oswal, K.C. Parmar, Synthesis and characterization of aliphatic-aromatic
1000 polyesters using interfacial polycondensation technique, Journal of Chemical and
1001 Pharmaceutical Research, 6 (2014) 705-714.
1002 [52] Y. Jin, Z. Su, Effects of polymerization conditions on hydrophilic groups in aromatic
1003 polyamide thin films, J. Membr. Sci., 330 (2009) 175-179.

[53] M.N. Abu Seman, M. Khayet, N. Hilal, Nanofiltration thin-film composite polyester polyethersulfone-based membranes prepared by interfacial polymerization, J. Membr. Sci., 348 (2010) 109-116.
[54] C.Y. Tang, Y.-N. Kwon, J.O. Leckie, Effect of membrane chemistry and coating layer on physiochemical properties of thin film composite polyamide RO and NF membranes: II. Membrane physiochemical properties and their dependence on polyamide and coating layers, Desalination, 242 (2009) 168-182.
[55] M. Jahanshahi, A. Rahimpour, M. Peyravi, Developing thin film composite poly(piperazine-amide) and poly(vinyl-alcohol) nanofiltration membranes, Desalination, 257 (2010) 129-136.

Table 1. Morphological and filtration properties of the unmodified supporting membranes: heat post-treatment temperature (T), heat post-treatment time (t), thickness (δ), weighted arithmetic mean of the nanofiber diameters ($\overline{\lambda_w}$) and its corresponding weighted standard deviation ($\overline{s_w}$), water contact angle (θ_w), void volume fraction (ε), mean pore size ($\overline{d_f}$) and pure water permeability (PWP).

Membrane	Heat treatment		Morphological properties					Filtration properties
	T (ºC)	t (min)	δ (μm)	$\overline{\lambda_w} \pm \overline{s_w}$ (μm)	θ_w (°)	ε (%)	$\overline{d_f}$ (nm)	PWP (LMH/bar)
ENM1	230	75	135 ± 19	0.76 ± 0.03	119.5 ± 1.8	80.6 ± 1.8	3220 ± 20	20248± 2151
ENM2	220	120	129 ± 20	0.73 ± 0.07	125.0 ± 2.6	79.3 ± 2.5	3084 ± 30	19914 ± 1801
PES	-	-	137 ± 14	-	26.8 ± 3.4	77.0 ± 7.0*	573 ± 3	15217± 1667

*Averaged data from Millipore supplier.

Table 2. Interfacial polymerization conditions used to prepare the polyester and polyamide thin film composite membranes.

Membrane	Support	TFC type[1]	Aqueous phase			Organic phase		
			Material[2]	w/w (%)	t_{ap}[3] (min)	Material[2]	w/v (%)	t_{IP}[3] (min)
PE TFNC1_5	ENM1	PE	BPA	2	60	TMC	0.25	5
PE TFNC1_10	ENM1	PE	BPA	2	60	TMC	0.25	10
PE TFNC1_15	ENM1	PE	BPA	2	60	TMC	0.25	15
PE TFNC1_20	ENM1	PE	BPA	2	60	TMC	0.25	20
PE TFNC2_15	ENM2	PE	BPA	2	60	TMC	0.25	15
PE TFC_15	PES	PE	BPA	2	60	TMC	0.25	15
PA TFNC1_5	ENM1	PA	PIP—TEA	1—1	60	TMC	0.25	5
PA TFC_5	PES	PA	PIP—TEA	1—1	60	TMC	0.25	5

[1]PE: polyester; PA: polyamide.
[2]BPA: bisphenol A; PIP: piperazine; TEA: triethylamine; TMC: trimesoyl chloride.
[3]$t_{ap:}$ aqueous phase time, t_{IP}: polymerization reaction time.

Table 3. Physicochemical properties and filtration performance of the unmodified supporting membranes and the polyester and polyamide thin film composite membranes: mean pore size ($\overline{d_f}$), zeta potential (ζ-potential), initial water permeate flux (J_{w_0}), mean humic acid (HA) permeate flux ($\overline{J_{HA}}$), final HA permeate flux (J_{HA_f}), mean HA separation factor ($\bar{\alpha}$), final HA separation factor (α_f), irreversible fouling factor (FR_w) and performance index (PI).

Membrane	Physicochemical properties		Filtration performance						
	$\overline{d_f}$ (nm)	ζ-potential * (mV)	J_{w0} $\left(10^2 \frac{kg}{m^2 h}\right)$	$\overline{J_{HA}}$ $\left(10^2 \frac{kg}{m^2 h}\right)$	J_{HAf} $\left(\frac{kg}{m^2 h}\right)$	$\bar{\alpha}$ (%)	α_f (%)	FR_w (%)	PI $\left(\frac{kg}{m^2 h}\right)$
ENM1	3220 ± 20	-59.4 ± 0.4	203 ± 22	9.3 ± 1.0	188 ± 20	39.1 ± 1.0	70.9 ± 0.4	96.8 ± 1.4	133 ± 14
ENM2	3084 ± 30	-63.2 ± 0.6	194 ± 19	13.7 ± 1.3	222 ± 18	29.3 ± 0.9	57.2 ± 0.6	98.5 ± 1.2	127 ± 10
PES	573 ± 6	-46.4 ± 0.1	152 ± 17	2.69 ± 0.30	117 ± 13	56.4 ± 1.4	84.0 ± 1.2	98.3 ± 1.3	98 ± 11
PE TFNC1_5	2868 ± 16	-59.9 ± 1.6	160 ± 17	6.94 ± 0.74	178 ± 19	42.4 ± 1.5	69.0 ± 1.5	93.3 ± 1.3	123 ± 13
PE TFNC1_10	2496 ± 88	-63.8 ± 0.8	3.5 ± 0.3	3.06 ± 0.17	117 ± 4	42.1 ± 1.4	70.3 ± 1.2	52.6 ± 4.8	82.4 ± 3.4
PE TFNC1_15	2255 ± 63	-72.5 ± 0.4	2.1 ± 0.2	1.51 ± 0.06	97.1 ± 3.7	42.3 ± 1.5	72.5 ± 1.2	10.2 ± 3.8	70.4 ± 2.9
PE TFNC1_20	827 ± 9	-70.2 ± 1.0	1.06 ± 0.04	0.26 ± 0.01	20.3 ± 0.8	61.6 ± 1.5	91.5 ± 1.2	22.9 ± 4.5	18.6 ± 0.7
PE TFNC2_15	1492 ± 30	-73.0 ± 1.0	0.99 ± 0.06	0.50 ± 0.02	42.5 ± 1.6	33.0 ± 1.6	62.5 ± 1.3	20.1 ± 5.0	26.6 ± 1.1
PE TFC_15	462 ± 4	-48.1 ± 1.2	0.26 ± 0.01	0.52 ± 0.02	79.1 ± 3.0	68.5 ± 1.3	86.9 ± 1.1	-220 ± 30**	68.7 ± 2.8
PA TFNC1_5	2844 ± 79	-49.2 ± 0.1	3.2 ± 0.2	2.89 ± 0.18	127 ± 6	36.4 ± 1.5	69.0 ± 1.3	46.4 ± 4.1	87.4 ± 4.7
PA TFC_5	521 ± 3	-34.8 ± 0.2	0.044 ± 0.002	0.057 ± 0.002	6.4 ± 0.2	70.1 ± 4.7	91.0 ± 1.1	-33.0 ± 8.0**	5.8 ± 0.2

*Values at pH=10; **The negative values of the FR_W are due to the partial detachment of the thin film layer from the supporting membrane.

Table 4. Peak assignments of the IR spectra of the unmodified supporting membranes and the polyester and polyamide thin film composite membranes.

Peak assignments	Wavenumbers (cm^{-1})	Polymers*	REF.
In-phase out-of-plane hydrogen deformation of para-substituted phenyl groups/Aliphatic C-H rocking	832, 853, 835, 858	PSU, PES	[20, 48]
Skeletal aliphatic C-C/aromatic hydrogen bending/ rocking	873, 1013, 1080, 1104, 1169, 872, 1011, 1073, 1104	PSU, PES	[20, 49]
C-SO_2-C symmetric stretching vibration	1148, 1148	PSU, PES	[20, 48,49]
C-O-C asymmetric stretching of aryl-O-aryl group	1237, 1239	PSU, PES	[20, 48,49]
S=O stretching vibration	1294, 1298	PSU, PES	[20, 48,49]
C-SO_2-C asymmetric stretching vibration	1322, 1321	PSU, PES	[20, 48,49]
C-H symmetric deformation of CH_3-C-CH_3 group	1364, 1387	PSU	[20, 48,49]
C=C aromatic in-plane ring stretching vibration	1409, 1407	PSU, PES	[20]
C-H stretching vibration of CH_3-C-CH_3 group	1486, 1485	PSU, PES	[20, 48,49]
C=C aromatic in-plane ring stretching vibration	1504, 1584, 1577	PSU, PES	[20, 48,49]
C-O stretching vibration of ester bonds (-COO-)	1200	PE	[29]
C=O stretching vibration of ester bonds (-COO-)	1720	PE	[6, 9, 29]
O-H stretching vibration of hydroxyl group (-OH) and carboxylic acid group (-COOH)	3355, 3393	PE	[6, 9, 50]
Stretching vibration of sulfonic group/C-O stretching vibration of ester groups	1027	PA	[48]
N-H in-plane bending coupled with C-N stretching/ C-H and N-H deformation vibration of amide bond formation (-CONH) (amide III band)	1283	PA	[46]
C-O stretching/O-H bending vibration of carboxylic acid/bending vibration of methylene group (-CH_2-)	1442, 1441	PA	[5, 10]
C-C and C-N in plane stretching vibration/ C=O stretching vibration of carboxylic acid salt	1584, 1580 (shoulder)	PA	[11, 12, 47]
C=O stretching/C-N stretching vibration of amide bond formation (-CONH) (amide I band)	1616, 1614 (peak) 1630, 1625 (shoulder)	PA	[5, 12, 16, 18, 47, 48]
C=O stretching vibration of carboxylic acid group	1697	PA	[5, 10, 47]
O-H stretching of carboxylic acid group (-COOH)/ N-H stretching vibration of residual amine groups	3426, 3393 (broad)	PA	[12, 13, 16, 17, 48]

*PSU: polysulfone; PES: polyethersulfone; PE: polyester; PA: polyamide. The colors are used to clarify the link between a specific wavenumber and its corresponding polymer.

Table 5. Interfacial polymerization conditions, physicochemical properties and filtration and antifouling performance of different reported polyester and polyamide thin film composite membranes: molecular weight cut off (*MWCO*), mean pore size (*MPS*), zeta potential (ζ-potential), transmembrane pressure (ΔP), pure water permeability (*PWP*), final separation factor (α_f) and irreversible fouling factor (FR_w).

Membrane[1] (monomer AP-monomer OP /support)	IP conditions[2]			Physicochemical properties		Filtration performance[3]				Antifouling performance[4]		Ref
	TFC type	AP/OP (% w/v)	t_{IP}	*MWCO* *MPS*	ζ-potential (mV) (pH)	ΔP (bar)	*PWP* (LMH/bar)	Solution	α_f (%)	Solution (pH)	FR_w (%)	
TEOA-TMC/PSU MF^{C}	PE	5/0.5^{oc}	35 min	-	-1.75* (9)	6	0.82*	0.6 g/L $MgSO_4$	56.8*	-	-	[29]
PEN-TMC/PES UF^{C}	PE	5/0.2^{oc}	20 min	820 Da	-57.4* (10)	5	1.3	1 g/L $MgSO_4$	67.9	-	-	[32]
(HPE-SDS)-TMC/PAN UF^{C}	PE	2.7-0.3/0.5	30 min	4000 Da	-14.1* (8)	6	6.2*	1 g/L $MgSO_4$	48.9*	-	-	[50]
TMBPA-TMC/PES NF^{C}	PE	0.1/0.15	30 sec	1.32 nm	-	6	4.6	-	-	15 mg/L HA (7)	5.4	[7]
BPA-TMC/PES NF^{C}	PE	2/0.15	10 sec	1.00 nm	-	6	2.6	-	-	15 mg/L HA (7)	-13.6*	[53]
TA-TMC/PES UF^{C}	PE	0.05/0.01^{oc}	3 min	-	-	2	23.4	1.2 g/L $MgSO_4$	50.2*	1 g/L HA	1.0	[8]
(SE-DMAP)-TMC/PES UF^{C}	PEA	1/0.05^{oc}	70 sec	474 Da	-43.2* (10)	5	6.0	1 g/L $MgSO_4$	83.9	0.5 g/L HA (7.4)	24.0	[6]
PIP-TMC/PES UF^{C}	PA	1/0.05^{oc}	70 sec	309 Da	-79.2 (9.8)	5	10.3	1 g/L $MgSO_4$	97.4	0.5 g/L HA (7.4)	48.0	
CDADO-TMC/PSU UF^{L}	PEA	2/0.3^{oc}	2 min	-	-23.3* (10)	10	5.3	2 g/L Na_2SO_4	91.0	0.5 g/L BSA	26.2	[5]
PIP-TMC/PSU UF^{L}	PA	2.5/0.3	2 min	-	-13.6* (10)	10	3.0	2 g/L Na_2SO_4	90.0	0.5 g/L BSA	58.6	
(PIP-BP-TEA)-TMC/PAN ENM^{L}	PA	0.7-0.3-1/0.1	1 min	-	-	4.8	20.4$_p$	2 g/L $MgSO_4$	87.0	-	-	[34]
(PIP-TEA)-TMC/PES ENM^{L}	PA	1-1/0.1	1 min	-	-	4.8	6.7$_p$	2 g/L $MgSO_4$	99.1	-	-	[33]
(PIP-TEA)-TMC/PAN UF^{C}	PA	1-1/0.1	1 min	-	-	4.8	3.0$_p$	2 g/L $MgSO_4$	97.3	-	-	
NF270^{C}	PA	-	-	-	-41.3 (9)	13.8	14.5	2 g/L $MgSO_4$	97.4	-	-	[33, 54]
NF90^{C}	PA	-	-	-	-37.0 (9)	13.8	11.2	2 g/L $MgSO_4$	99.0	-	-	
(PIP-DABSA)-TMC/PAN MF^{L}	PA	1-1/0.1^{oc}	1 min	-	-	3	20.4*	1 g/L Na_2SO_4	95.6*	1.5 g/L CTAB	15.4	[10]
PIP-TMC/PAN MF^{L}	PA	2/0.1	1 min	-	-	3	15.2	1 g/L Na_2SO_4	95.2*	1.5 g/L CTAB	46.7	
PIP-TMC/PSU UF^{L}	PA	2/0.05	30 sec	294* Da	-28.9* (6.5)	7	4.1$_p$	2 g/L $MgSO_4$	89.6	1 g/L BSA (7.4)	16.0	[4]
PIP-TMC/PSU UF^{L}	PA	0.2/0.15	50 sec	280 Da	-65.2 (7)	5	14.2	0.5 g/L Na_2SO_4	98.3	0.5 g/L BSA (7)	24.8	[3]
BPA-TMC/PSU ENM^{L}	PE	2/0.25^{oc}	15 min	2.26 μm	-72.5 (10)	1	213	15 mg/L HA	72.5	15 mg/L HA (11)	10.2	This study
BPA-TMC/PES MF^{C}	PE	2/0.25	15 min	0.46 μm	-48.1 (10)	1	25.6	15 mg/L HA	86.9	15 mg/L HA (11)	-220**	
(PIP-TEA)-TMC/PSU ENM^{L}	PA	1-1/0.25	5 min	2.84 μm	-49.2 (10)	1	324	15 mg/L HA	69.0	15 mg/L HA (11)	46.4	
(PIP-TEA)-TMC/PES MF^{C}	PA	1-1/0.25	5 min	0.52 μm	-34.8 (10)	1	4.4	15 mg/L HA	91.0	15 mg/L HA (11)	-33.0**	

[1]AP = aqueos phase; OP = organic phase; ^{C} = comercial support; ^{L} = Lab-made support; TEOA = triethanolamine; TMC = trimesoyl chloride; PSU = polysulfone; MF = microfiltration; PEN = pentaerythritol; PES = polyethersulfone; UF = ultrafiltration; HPE = hyperbranched polyester; SDS = sodium dodecyl sulfate; PAN = polyacrylnitrile; TMBPA = tetramethyl bisphenol A; NF = nanofiltraton; BPA = bisphenol A; TA = tannic acid; SE = seriol (2-Amino-1, 3propanediol); DMAP = 4-dimethylaminopyridine; PIP = piperazine; CDADO = carboxylated aromatic diamine-diol; BP = bipiperidine; TEA = trimethylamine; ENM = electrospun nanofiber membrane; DABSA = 2,5-diaminobenzene sulfonic acid.

[2]IP = interfacial polymerization; PE = polyester; PEA = polyesteramide; PA = polyamide; ^{oc} = optimized conditions; t_{IP} = IP reaction time.

[3]The subscript p indicates that these values correspond to permeate fluxes instead of pure water fluxes.

[4]HA = humic acid; CTAB = cyltrimethylammonium bromide; BSA = bovine serum albumin.

*Estimated values taken from figures plotted in the corresponding reference.

**The negative values of the FR_w are due to the partial detachment of the thin film layer from the supporting membrane.

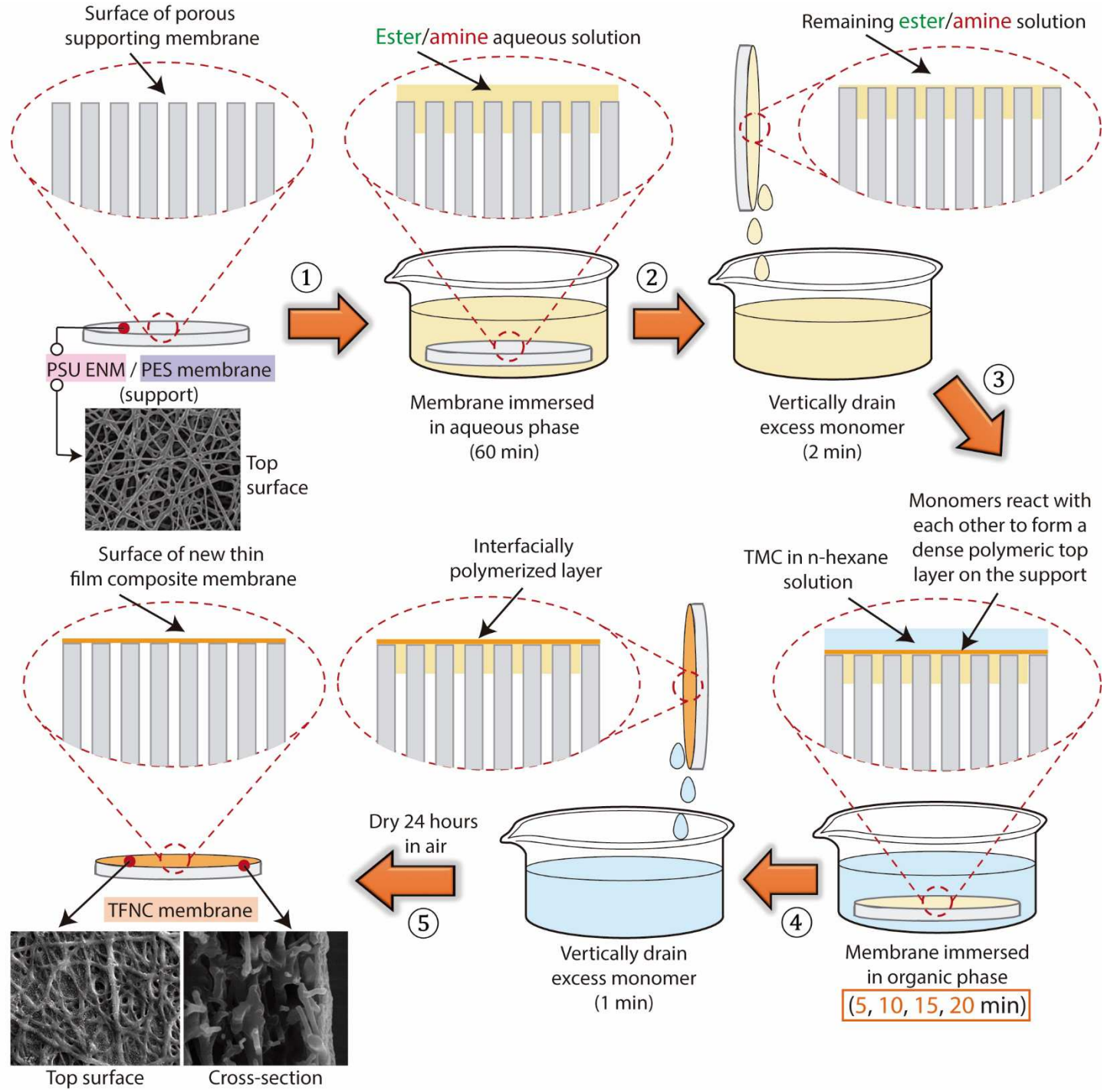

Figure 1. Schematic illustration of the preparation process of polyester and polyamide thin film composite membranes by interfacial polymerization.

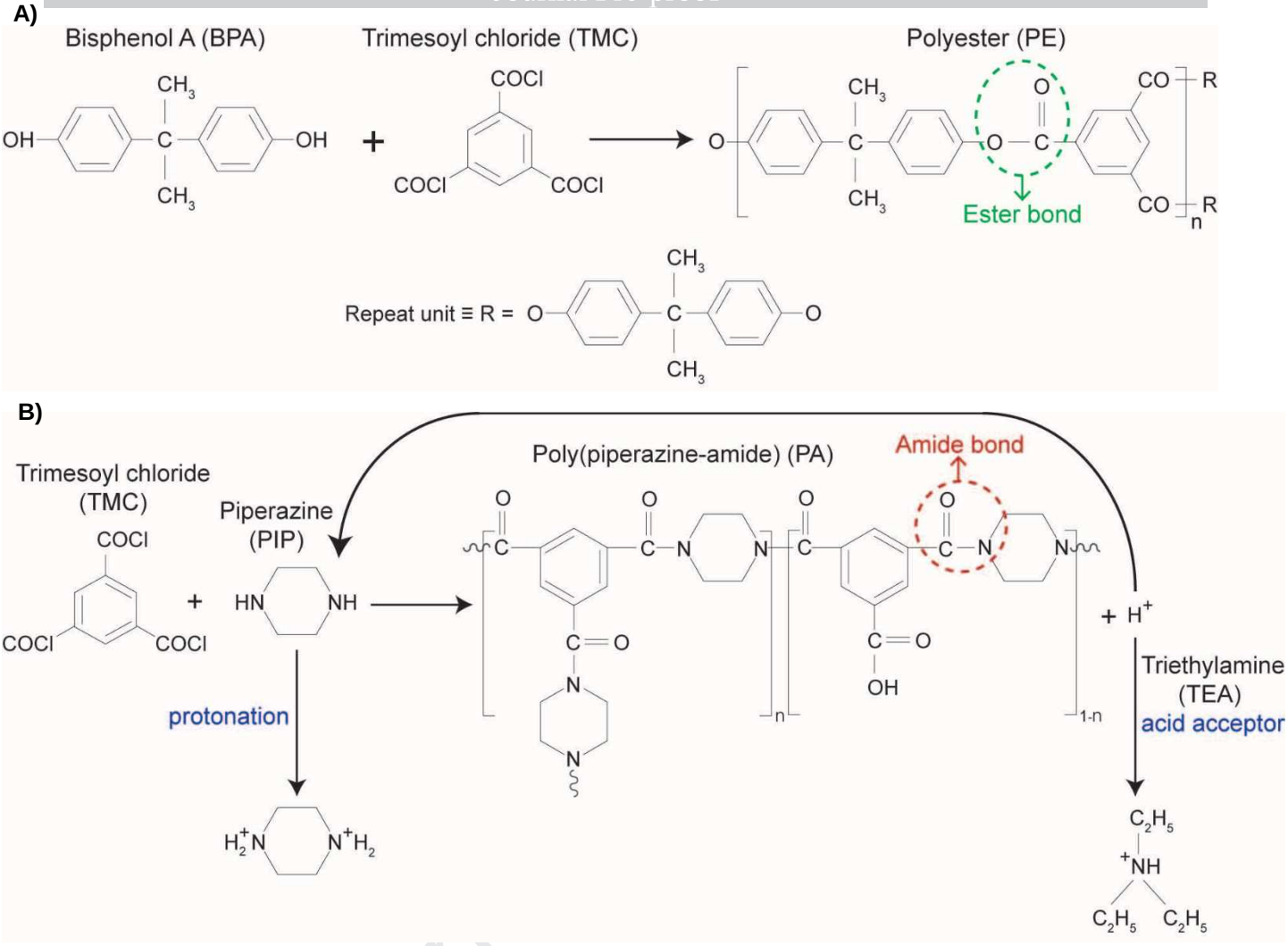

Figure 2. **Schematic of the interfacial polymerization reaction of different monomers. A)** Bisphenol A and trimesoyl chloride react to form polyester (PE) and **B)** piperazine and trimesoyl chloride in presence of acid acceptor triethylamine to form polyamide (PA).

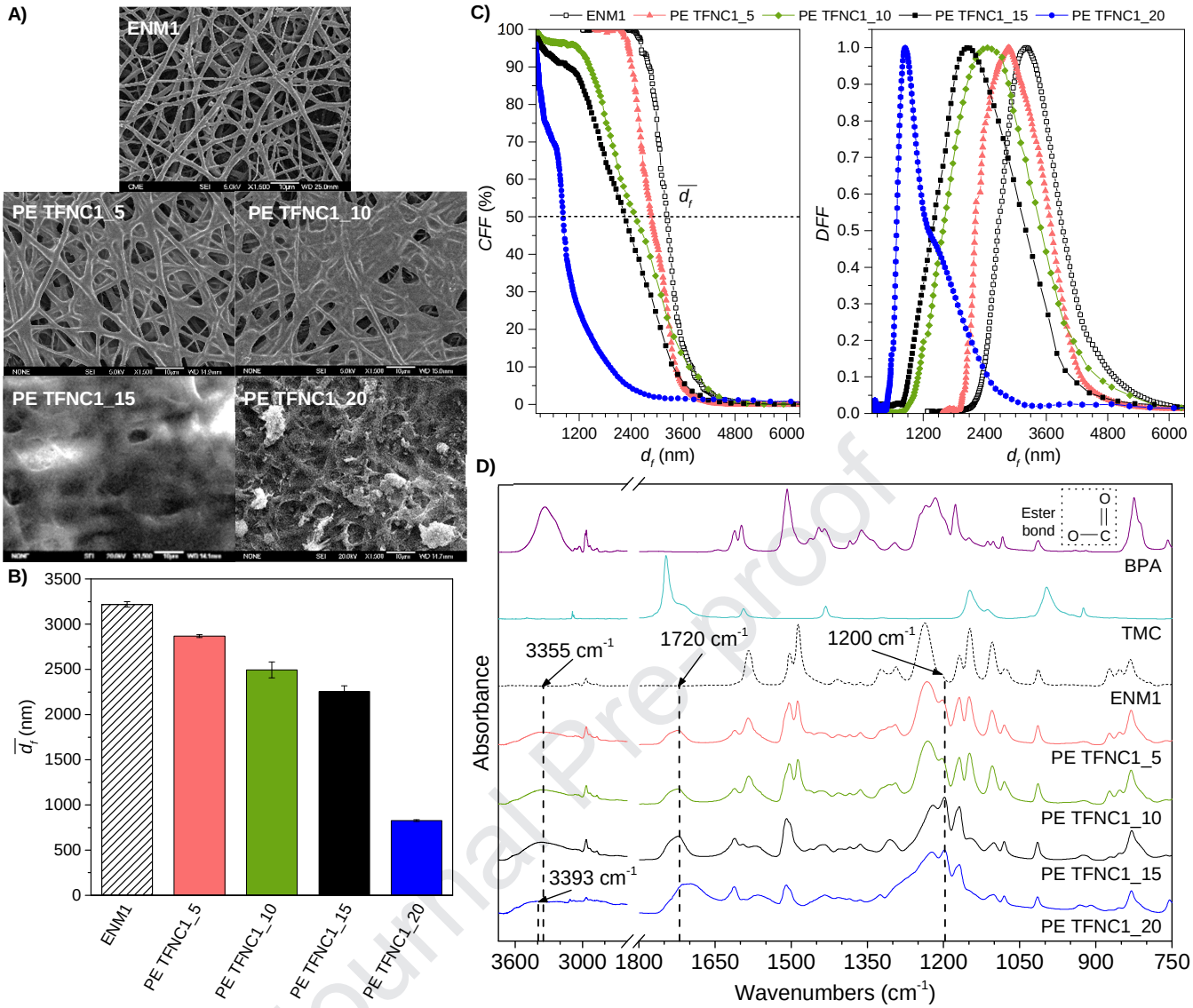

Figure 3. Influence of the polymerization reaction time on the morphological and structural characteristics of polyester thin film nanofiber composite membranes. A) SEM surface images at X1500 magnification, **B)** mean pore size ($\overline{d_f}$), **C)** normalized differential (DFF) and cumulative (CFF) pore size distributions, and **D)** FTIR spectra of the unmodified supporting membrane (ENM1) and the surface modified PE TFNC membranes prepared with reaction times of 5 min (PE TFNC1_5), 10 min (PE TFNC1_10), 15 min (PE TFNC1_15) and 20 min (PE TFNC1_20). The PE TFNC membranes were prepared by reacting BPA and TMC as described in Fig. 2A.

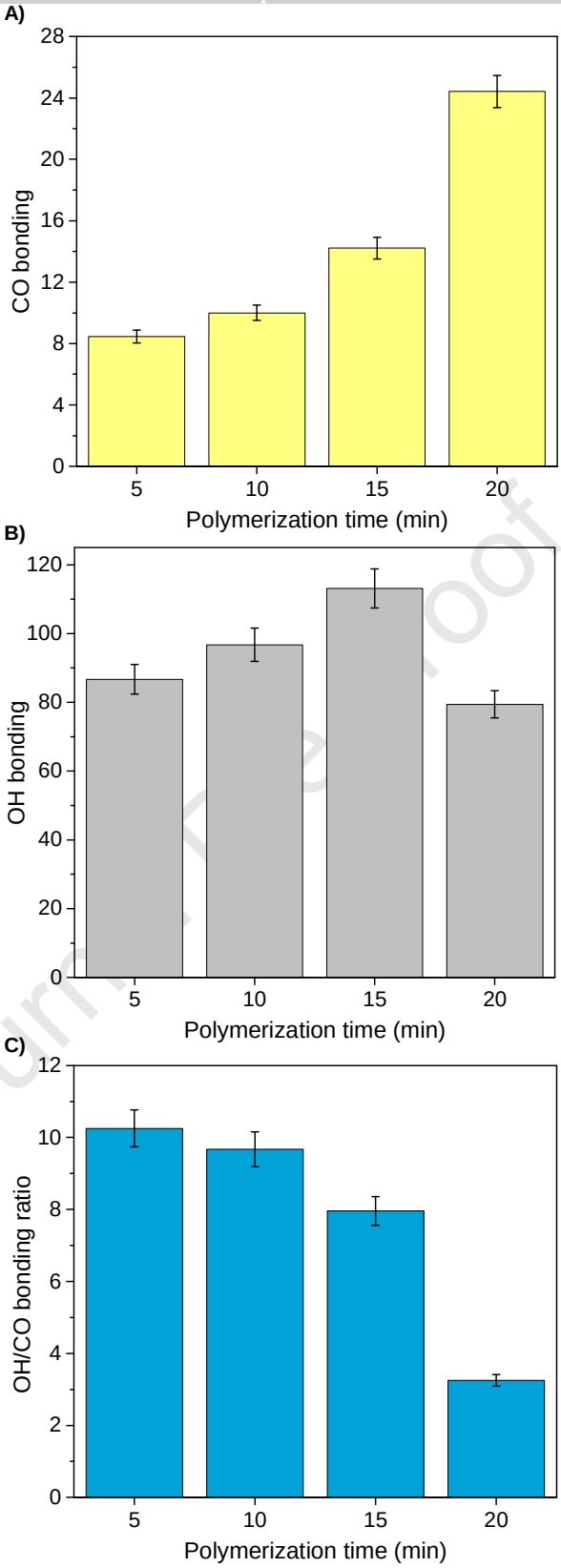

Figure 4. Influence of the polymerization reaction time on the bondings and bonding ratio of polyester thin film nanofiber composite membranes. A) Area under the peak at 1720 cm^{-1} corresponding to the –C=O fuctional group (i.e. CO bonding), **B)** area under the peak at 3355 cm^{-1} corresponding to the –OH fuctional group (i.e. OH bonding), and **C)** area bonding ratio of these two functional groups (i.e. OH/CO).

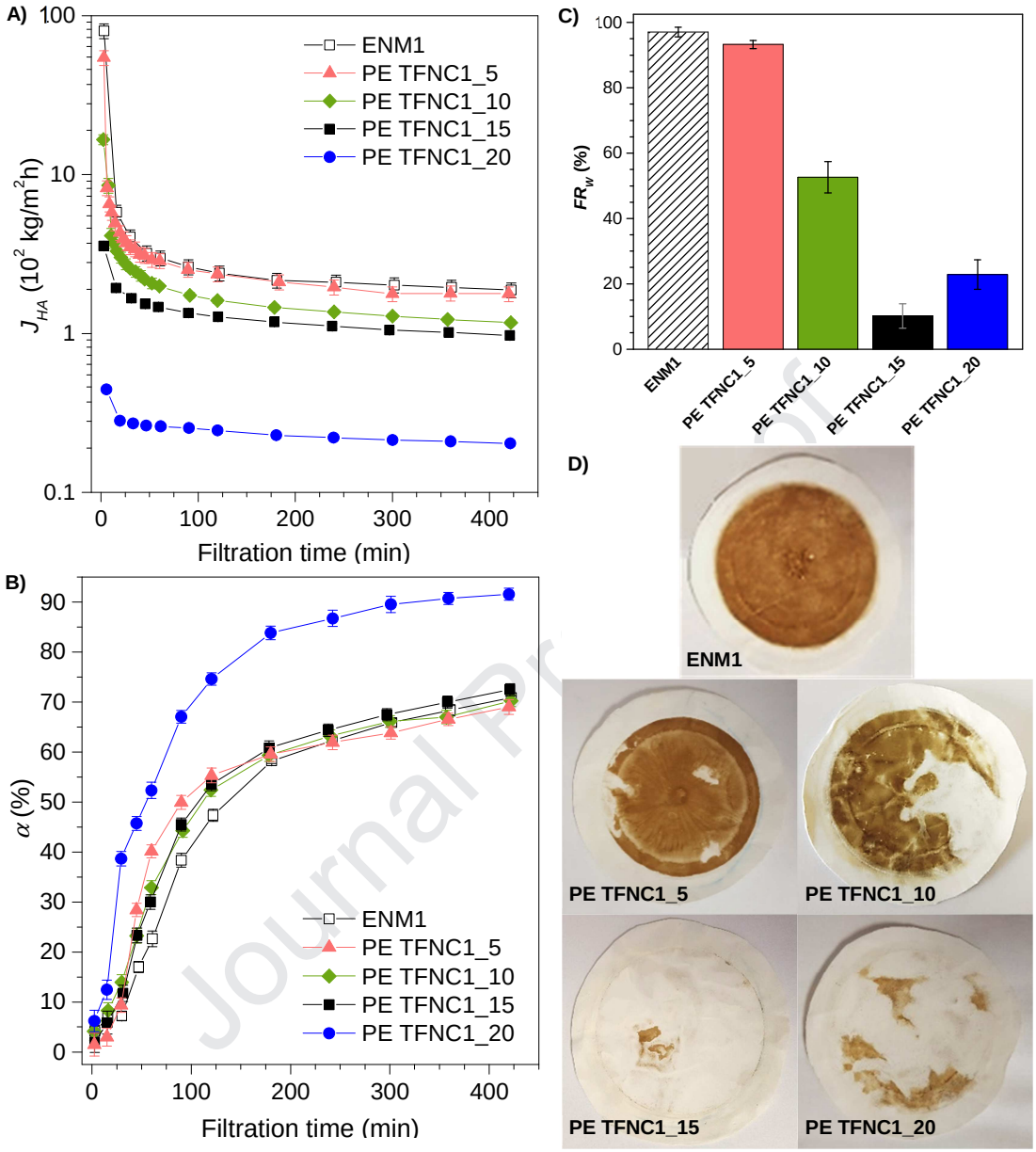

Figure 5. Influence of the polymerization reaction time on the filtration properties of polyester thin film nanofiber composite membranes. A) Humic acid permeate flux (J_{HA}) and **B)** separation factor (α) as a function of filtration time of the unmodified supporting membrane (ENM1) and the surface modified PE TFNC membranes prepared with reaction times of 5 min (PE TFNC1_5), 10 min (PE TFNC1_10), 15 min (PE TFNC1_15) and 20 min (PE TFNC1_20). **C)** Irreversible fouling factors (FR_W), and **D)** photographs of the membranes after the filtration tests carried out with 15 mg/L HA feed aqueous solution at pH 11 and 10^5 Pa transmembrane pressure.

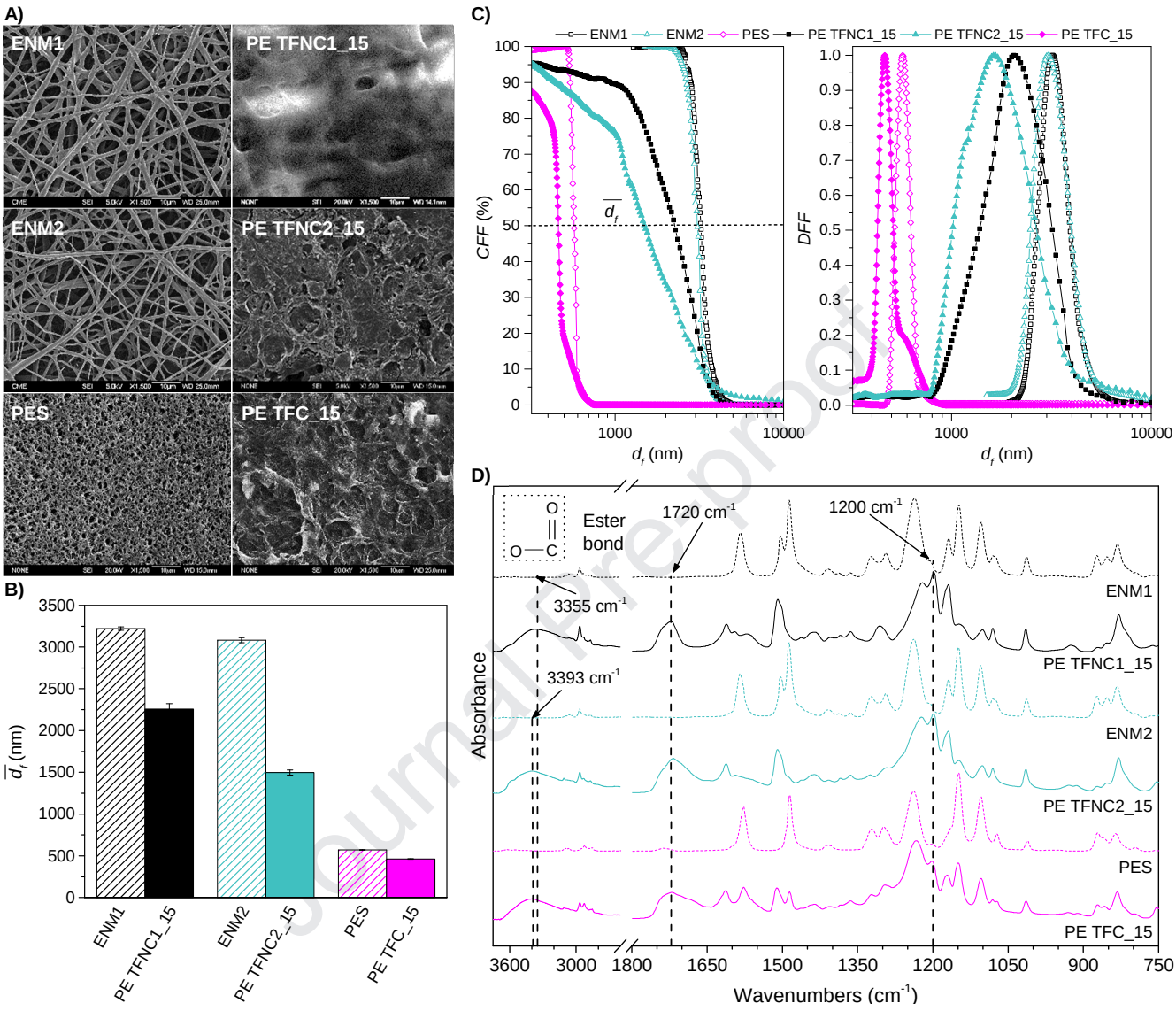

Figure 6. **Influence of the supporting membrane on the morphological and structural characteristics of polyester thin film composite membranes. A)** SEM surface images at X1500 magnification, **B)** mean pore size ($\overline{d_f}$), **C)** normalized differential (DFF) and cumulative (CFF) pore size distributions, and **D)** FTIR spectra of the unmodified supporting membranes (ENM1, ENM2, PES) and the surface modified membranes (PE TFNC1_15, PE TFNC2_15, PE TFC_15, respectively). All membranes were prepeared with 15 min reaction time of BPA and TMC as described in Fig. 2A.

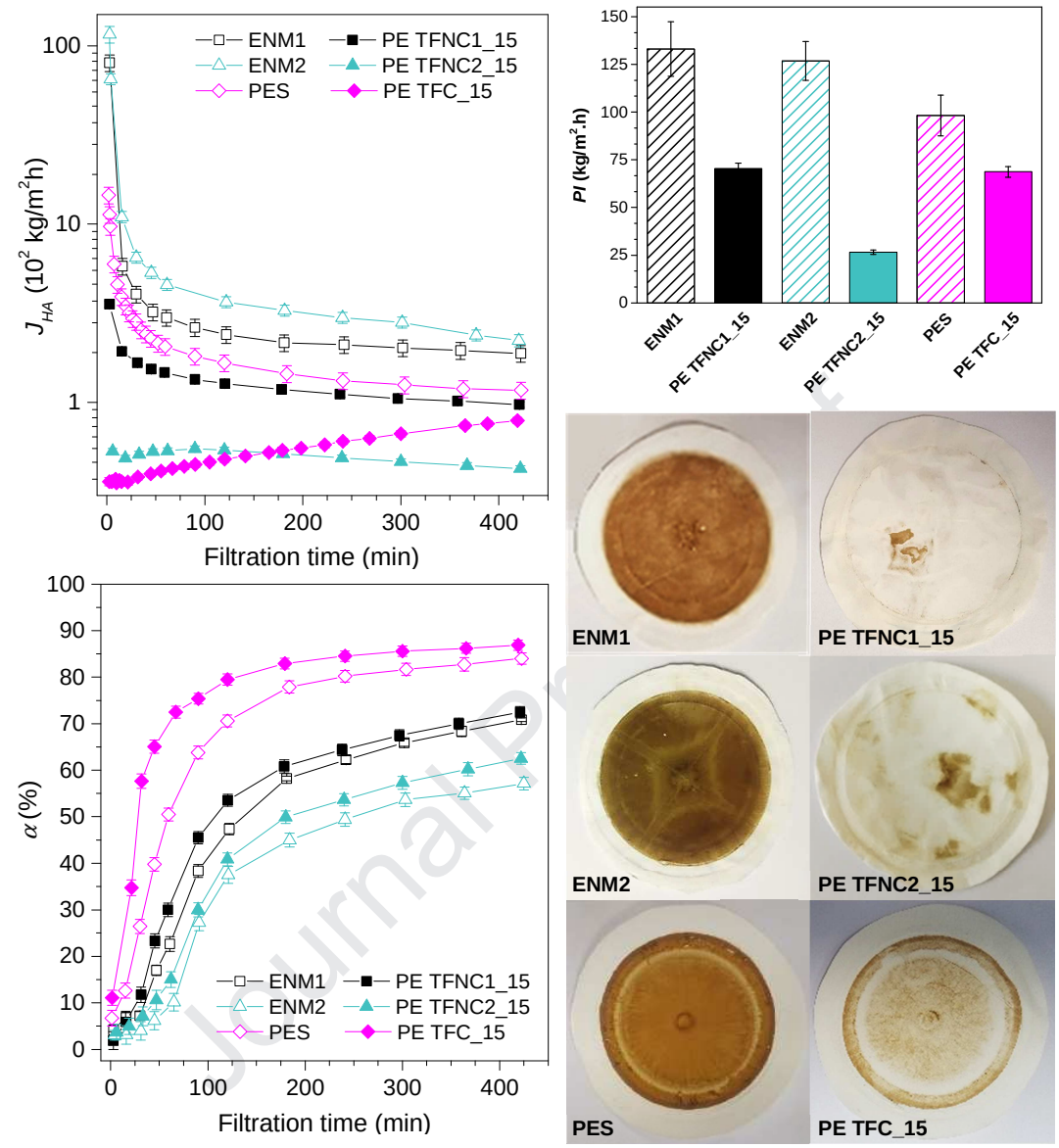

Figure 7. **Influence of the supporting membrane on the filtration properties of polyester thin film composite membranes**. **A)** Humic acid permeate flux (J_{HA}) and **B)** separation factor (α) as a function of filtration time of the unmodified supporting membranes (ENM1, ENM2, PES) and the surface modified membranes (PE TFNC1_15, PE TFNC2_15, PE TFC_15, respectively). **C)** Performance index (*PI*) and **D)** photographs of the membranes after filtration tests carried out with 15 mg/L HA feed aqueous solution at pH 11 and 10^5 Pa transmembrane pressure.

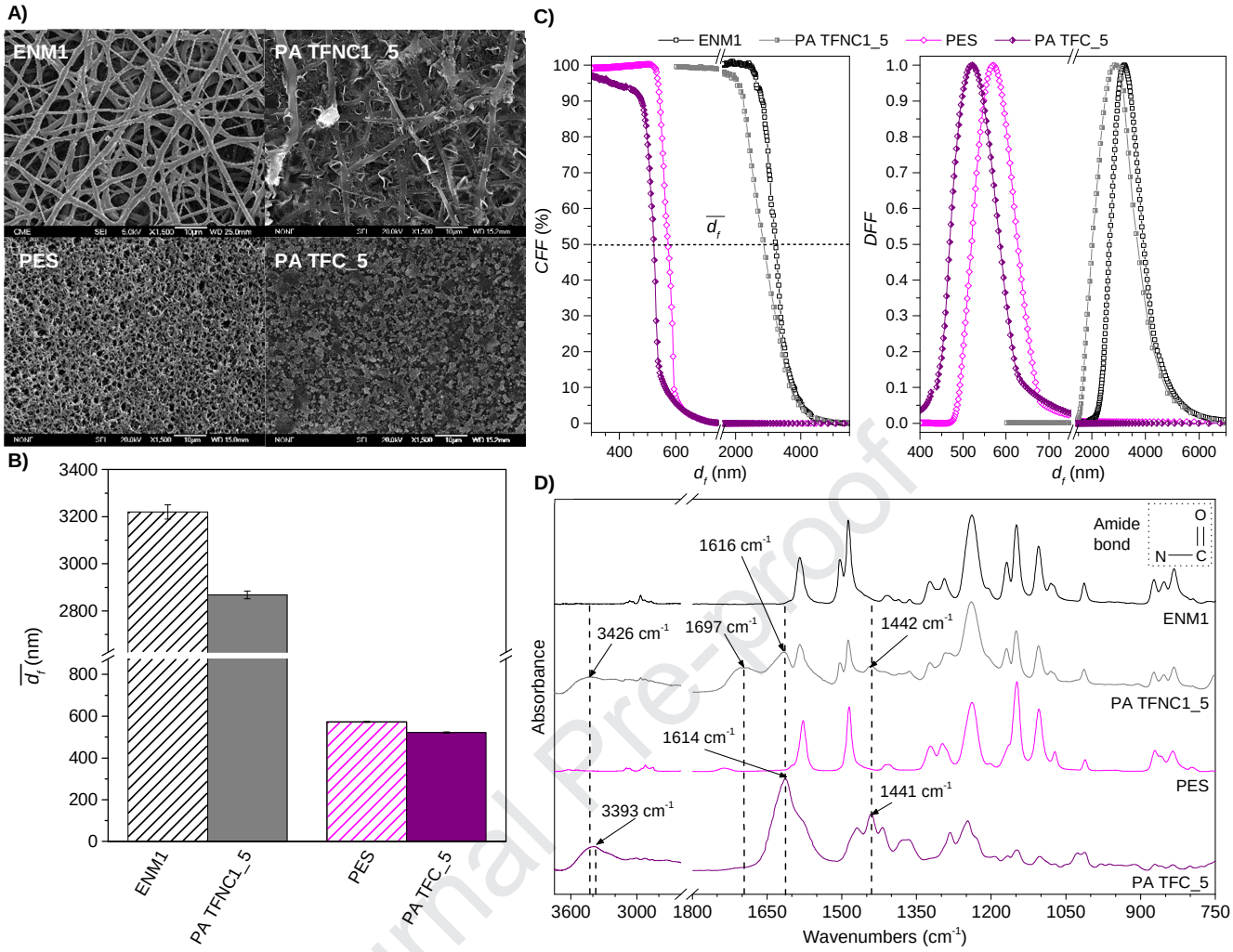

Figure 8. Morphological and structural characteristics of polyamide thin film composite membranes prepared on different supports. A) SEM surface images at X1500 magnification, **B)** mean pore size ($\overline{d_f}$), **C)** normalized differential (DFF) and cumulative (CFF) pore size distributions, and **D)** FTIR spectra of the unmodified supporting membranes (ENM1, PES) and their respective surface modified membranes (PA TFNC1_ 5, PA TFC_5). The PA TFC membranes were prepared with 5 min reaction time of PIP and TMC in presence of the acid acceptor TEA as described in Fig. 2B.

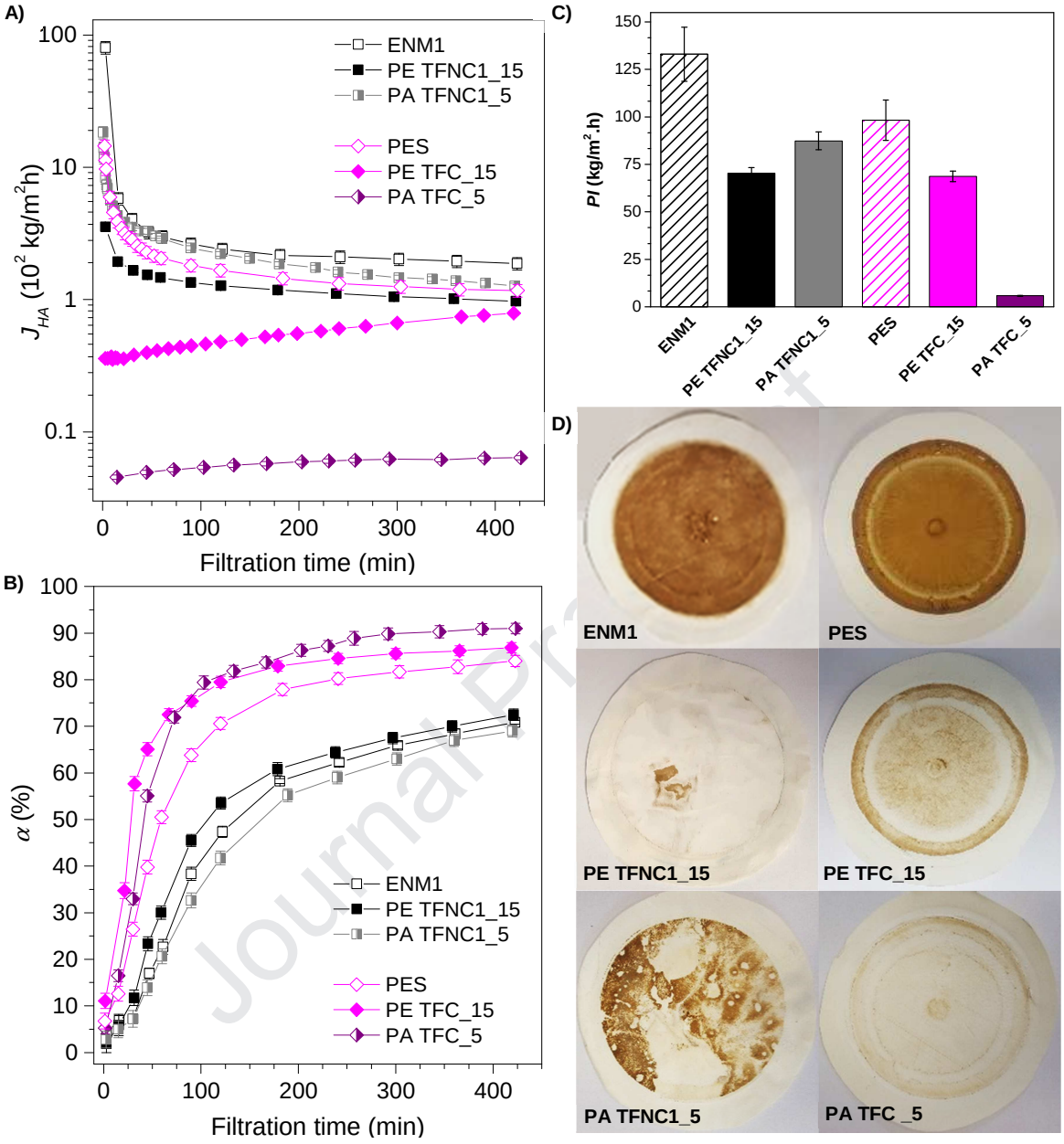

Figure 9. Comparison of the filtration properties of polyester and polyamide thin film composite membranes prepared on different supports. A) Humic acid permeate flux (J_{HA}) and **B)** separation factor (α) as a function of filtration time of the unmodified supporting membranes (ENM1, PES) and their respective surface modified polyester (PE TFNC1_15, PE TFC_15) and polyamide (PA TFNC1_5, PA TFC_5) TFC membranes. **C)** Performance index (*PI*), and **D)** photographs of the membranes after the filtration tests carried out with 15 mg/L HA feed aqueous solution at pH 11 and 10^5 Pa transmembrane pressure.

Highlights

Polyester (PE) and polyamide (PA) layers prepared by interfacial polymerization (IP)

Use of different supports to prepare PE and PA thin film composite (TFC) membranes

Study of the effect of IP reaction time on PE membrane antifouling performance

Relation between physicochemical, filtration and antifouling properties of membranes

Comparison of filtration and antifouling performance of PE and PA TFC membranes

Declaration of interests

☒ The authors declare that they have no known competing financial interests or personal relationships that could have appeared to influence the work reported in this paper.

☐The authors declare the following financial interests/personal relationships which may be considered as potential competing interests: